JETI Journal of Emerging Technologies and Innovations

JETI | Vol. 1 No. 1 (2024)

PAPER

Optimizing Conditions for the Discharging of Lithium-ion Batteries catalyzed by Zinc Powder through Response Surface Methodology

Karlo Isagani A. Mosqueda

Master in Engineering – Chemical Engineering, Professional Schools
University of Mindanao, Matina, Davao City, Philippines

k.mosqueda.375722@umindanao.edu.ph

ABSTRACT

This study aims to optimize the discharging process of lithium-ion batteries (LIBs) using zinc powder as a catalyst and NaCl solution as an electrolyte through Response Surface Methodology (RSM). Experiments were conducted to examine the effects of NaCl concentration (9.27–22.73%), discharging time (49.77–100.23 minutes), and Zn-NaCl ratio (0.39–2.41%) on key response variables: Percent Voltage Drop (53.42–59.32%), Residual Voltage Percent (40.68–47.79%), and Discharge Rate (0.020–0.038 V/min). A Central Composite Design (CCD) was employed to develop predictive models and analyze variable interactions. Statistical analyses revealed that higher NaCl concentrations, extended discharging times, and moderate Zn powder ratios significantly improved the discharging process, ensuring lower residual voltages and faster discharge rates. Optimal criteria for conditions included 20% NaCl concentration, 90 minutes of discharging, and 2.0% Zn powder ratio, achieving a predicted response (corresponding an actual response in Run 15): 57.197% (56.22%) voltage drop; 42.803% (43.78%) residual voltage; and 0.021 V/min (0.021 V/min) with a desirability of 0.846 or 84.6%). The predicted and actual response values closely align, confirming that the optimized discharging parameters effectively ensure the safe and efficient preparation of LIBs for recycling, minimizing risks posed by residual energy. Future studies could investigate alternative catalysts and assess the scalability of the process for industrial applications.

KEYWORDS

Lithium-ion battery discharging optimization; Lithium-ion Battery Recycling; Response Surface Methodology (RSM); Residual voltage reduction in LIB recycling; Central Composite Design (CCD)

1 INTRODUCTION

Lithium-ion batteries (LIB) are secondary (or rechargeable) batteries wherein the lithium ions move from the cathode to the anode during charging and vice versa when discharging [1]. LIBs are primarily used in consumer electronics [2], such as mobile phones and laptops [3]. In recent years, however, the LIB industry has also penetrated the electronic vehicle (EV) industry. The emergence of LIBs as a dominant force in different industries is due to their superior energy density, high voltage increased storage life, wide operating temperature, and low discharge rate when not in use [4].

One specific type of LIB is Lithium Cobalt Oxide (LCO) or LiCoO2. This is the first commercial iteration of this battery which was developed in 1980, and Sony used lithiated cobalt oxide active material to commercially produce and market LIBs in 1991 [5]. A LIB is commonly made up of five (5) components: the cathode, the anode, the electrolyte, the separator, and the current collectors [6]-[7].Common materials used cathodes include LCO[8], lithium nickel cobalt manganese oxide[9], lithium-ion phosphate [10]-[11], including electronic conducting polymers [12]-[13]. Anodes in LIB are usually made up of carbon-based (i.e., CNTs, graphene, graphite [14]), silicon-based compounds [15]-[16], alloy materials [17], and transition metal oxides [18]. Electrolytes used in LIB include LiPF6 [19], LiClO4 [20], and LiCF3SO3 [21].

Several recycling methods are available for extracting lithium and cobalt from spent secondary batteries, such as hydrometallurgical, pyrometallurgical, and direct physical recycling [22]. This includes hydrometallurgical processes such as leaching and reduction using inorganic acids [23]-[25] and organic acids [22], [26]-[27]. Pyrometallurgical recycling is another method of extracting lithium and cobalt from spent LIBs which involves the successive preheating, pyrolysis, and smelting of LIBs [28]. Direct physical recovery, on the other hand, is a process where precious components (e.g., Li/Co, etc.) are extracted without the use of chemicals or mechanical means [29]-[30].

The efficiency of the overall LIB recycling process is increased through pre-treatment, which includes mechanical and/or chemical methods [31]-[32]. One important part of the pre-treatment process is the discharging of spent LIBs. During the dismantling process of spent LIBs, short-circuiting and spontaneous combustion may occur due to the remaining power in the LIB [33] and may release stored chemical energy [22]. It was reported that 65% of fire incidents from waste plants in the state of California are caused by the rapid release of energy (which can lead to fires and explosions) from LIBs not fully discharged [34]. The optimized discharging of spent LIBs facilitates the avoidance of these dangerous incidents.

Several studies are available on the discharging of spent LIBs. One popular approach to discharge spent LIBs is to immerse the battery in salt solutions [35]-[36]. Due to the lack of consensus on the optimum electrochemical solution for the discharging process, one study employed different salts (i.e., NaCl, Na2S, and MgSO4) at different concentrations (12-20%) and conditions (i.e., temperature and ultrasonication) to discharge mobile phone battery. The results showed that NaCl had the best results when it came to discharging the LIBs. The results in varying the temperature displayed no significant difference, but the ultrasonication of the setup exhibited positive results as it reduced the discharging time to less than two (2) hours because of the effect of the ultrasonic waves on the formation of sediments. Corrosion was also a problem in the electrodes (copper wires) used in the process. This can be addressed using corrosive-resistant electrodes, preferably stainless steel, as other options, such as platinum and silver electrodes, can be costly [37].

The addition of metal catalysts as sacrificial metal helps in significantly decreasing the discharging time. The introduction of Zn and Fe as metal catalysts in 20% NaCl solution has reduced the complete discharging of batteries from 4.4 hours to 0.25-0.32 hours [38], but no optimized conditions for these factors are available. This predicament calls for optimizing the discharging of spent LIBs using zinc powder as a catalyst through response surface methodology (RSM). The optimization of catalyst dosages such as zinc is vital because (1) excess Zn as a catalyst may lead to higher costs without so much affecting the discharging process, and (2) inadequate Zn may lead to an incomplete reaction which limits the electrons transfer and lead to longer discharging times.

Response Surface Methodology (RSM) is a statistical approach that is frequently used for complex system modeling and optimization. RSM is especially helpful in the presence of several variables and when the relationship of these variables is nonlinear. In RSM, an optimal combination of input variables is identified to yield the desired response [39]-[41]and is used in various processes in different disciplines[42]-[44].

Advantages over other optimization methods include: (1) Reduces the number of experiments (or trials) since RSM can model the response surface and predict the response with few experiments; (2) Provides information on the influence of independent variables, which can be used to understand the input and response variables further and consequently identify the critical factors affecting the responses; (3) Identify the optimal setting for the independent variables (input) that can maximize the response variables in interest; and (4) Provides information on the interaction and relationship of the independent and response variables which helps in understanding the effects of the independent variables on the response[45]-[47].

This study mainly aims to optimize the discharging process in LIBs using zinc powder as a catalyst using response surface methodology, providing discharged batteries that are ready and safe for further recycling processes. Specifically, it aims to (1) produce a Design of Experiment (DoE) with (a) NaCl Concentration (%), (b) time (in mins), and (c) Zn Powder in NaCl Solution (%) as independent variables and describe the voltage profile for the experimental run; (2) analyze the relationship of the variables and understand its impact in the discharging optimization through statistical model; (3) formulate a mathematical model for the response variables: Percent Voltage Drop Er, Residual Voltage Percent Et, and Discharge Rate Ed using Design-Expert®; and (4) validate the actual model equations by exploring optimization studies provided by the software.

The study is vital in providing completely discharged LIBs safe from possible dangers such as spontaneous combustion, short-circuiting, and explosion. Furthermore, the findings in this study will add to the existing body of knowledge on optimizing the discharging process in spent LIBs.

This research is limited to using 18650-type LIBs in the discharging process, which will be placed in a jig to secure the set-up while the process is ongoing. Using RSM, the factors (input variables) will include the following: (1) Concentration of NaCl as Electrolyte, which impacts the ionic conductivity of the electrolyte, balancing low mobility and unwanted side reactions; (2) Discharging Time, which determines the extent of residual energy depletion and operational costs; and (3) Zinc Powder Ratio with NaCl electrolyte, which enhances electron transfer efficiency as a catalyst.

Meanwhile, the response variable is the residual voltage percentage Et; percentage voltage drop Er; and Discharge Rate Ed. Voltage drop is measured to determine how much energy is successfully dissipated, ensuring that the battery is neutralized before recycling. Residual voltage is quantified for safety, as it measures the remaining stored energy, preventing potential hazards such as short circuits or thermal runaway. The discharge rate is assessed to understand how quickly the battery loses voltage, which is essential for optimizing process time and ensuring that the discharging method is both practical and scalable for industrial applications.

The Data Acquisition and Control Interface (DACI) is employed to read voltage Vt at time t and graph the data for the study. The experimental design, utilizing Response Surface Methodology (RSM), is conducted through Design-Expert® software, specifically using the Central Composite Design (CCD).

2 MATERIALS AND METHODS

2.1 Materials and Resources

To ensure repeatability, all the batteries used in this study are 18650-types with an initial voltage of ~3.7V. The number of batteries that will be used for the discharging trials is based on the number of input variables in the Design-Expert® software. A discharging jig (Figs. 2 and 3) is used for the process and has stainless steel electrodes (SS316L). The reagents in the study include NaCl (Technical Grade; Chem Vest Commercial Trading) as electrolyte and Zn powder

(Analytical Grade, 95%; Techno Pharmchem India) as metal catalyst. A Data Acquisition and Control Interface (DACI) used in complementary with the Low Voltage DC and AC Electrical Machines Software (LVDAC-EMS) are used for the recording of real-time data for the voltage of the discharging process.

2.2 Preliminary and Benchmark experiments

Studies on the use of metal-catalyzed electrolytes in the discharging of LIBs, although already present, lack details on the optimum S/L ratio for the Zn powder and NaCl solution (S/L Ratio). Therefore, it is vital that baseline numerical data on the S/L ratio of the Zn powder to the NaCl solution is established as one of the independent variables determined for the discharging optimization. The basis for the other numerical input variables (i.e., NaCl Concentration and Time) are based on studies conducted by M. M. Torabian, M. Jafari, and A. Bazargan [33]. Table 1 shows the summary of the benchmark discharging experiments as the basis for the S/L ratio of the Zn powder and NaCl Solution.

Aside from numerical input variables, categorical variables were also considered, such as the agitation of the slurry to ensure the availability of Zn powder as a catalyst in proximity to the electrodes. The benchmark experiment is shown in Table 2.

Table 1. Conditions for the Benchmark experiments on S/L ratio.

Runs	[NaCl], %	S/L Ratio, %	Time, mins
1	20	0.5	120
2	20	1.0	120
3	20	1.5	120
4	20	2.0	120
5	20	3.0	120
6	20	5.0	120

Table 2. Benchmark experiments for agitation through magnetic stirring.

Runs	[NaCl], %	S/L Ratio, %	Time,	Agitation
1	20	0.5	120	Not Stirred
2	20	0.5	120	Stirred
3	20	1.0	120	Not Stirred
4	20	1.0	120	Stirred

2.2 Setting up the Design of Experiment (DoE) through Design-Expert® using Central Composite Design (CCD)

The Central Composite Design (CCD), the most common response surface, will be used in the DoE using Design-Expert®. CCD is based on a factorial design that has both central points and axial points to examine variables at three levels, thus enabling correct estimation of the quadratic terms for the response. The experimentation required from the information of an accurately planned factorial experiment makes CCD suitable as the DoE of this study [47]. The input (independent) variables in this study about the CCD using Design-Expert® are: (1) Concentration of NaCl as Electrolyte, A; (2) Discharging Time, B; and (3) Zinc Powder Ratio with NaCl electrolyte (S/L Ratio), C. The response variables are: (1) percentage voltage drop Er; (2) residual voltage percent Et; and (3) Discharge Rate Ed.

In setting up the DoE through the Design-Expert® software using CCD, the input variables' factor levels (i.e., high, low, center). The highs and lows for the NaCl Concentration and Time are based on the results of the study conducted by M. M. Torabian, M. Jafari, and A. Bazargan [33]. Consequently, the high and low values for the S/L ratio and the inclusion of agitation as a categorical variable are based on the benchmark experiments conducted in preparation for setting up the DoE.

2.3 Design and Fabrication of Discharging Jig

A discharging jig was designed and fabricated using a plastic container that can house three (3) sets of discharging set-ups holding four (4) 18650 Batteries, as shown in Fig. 1. The electrodes used in the discharging jig are SS316L Stainless Steel to address possible corrosion issues despite the external discharging setup.

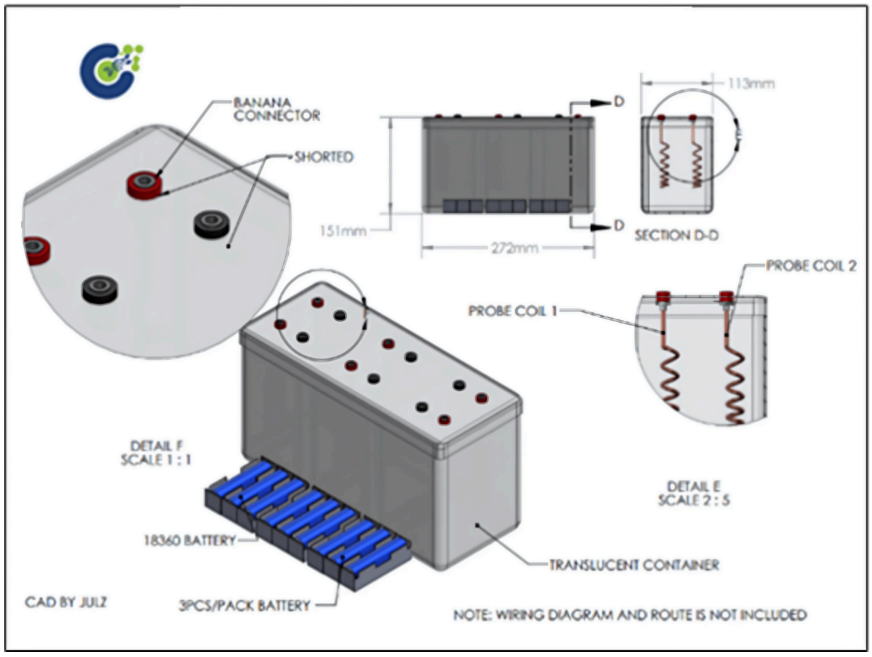

Fig. 1 Proposed design for the discharging optimization of 18650-type Li-ion batteries.

2.4 Electrolyte and Catalyst Preparation

A stock solution of 20% NaCl solution is prepared using rock salt and deionized water. Once completely dissolved, it was filtered to extract the unwanted particles that could affect the discharging process. The solution was diluted as specified by the DoE generated by the Design-Expert® software. Zinc Powder-NaCl Solution (S/L ratio) was also prepared in compliance with each experimental run generated by the Design-Expert® software. The Zinc Powder in the NaCl Solution mixture is then transferred into the jig to prepare for discharging. The connection of the discharging jig to the DACI is set according to Fig. 2.

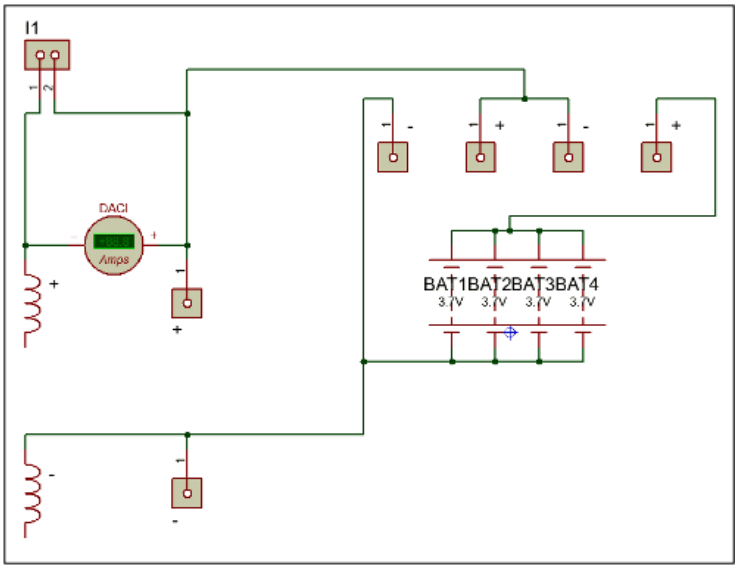

Fig. 2 Schematic diagram from Proteus for the Discharging setup using DACI.

2.5 Discharging Optimization Process

Upon completing the set-up, the discharging process is recorded through the reading of voltage in real-time by DACI. This reading is also recorded and is graphed automatically in the computer connected to DACI through the LVDAC-EMS software. Fig. 3 shows that three groups of four 18650 batteries are in a holder and can be simultaneously discharged. However, for the study, it will only be discharging one battery per holder which would total three batteries at a time, representing the number of replicates per experimental run that will be produced by the DoE.

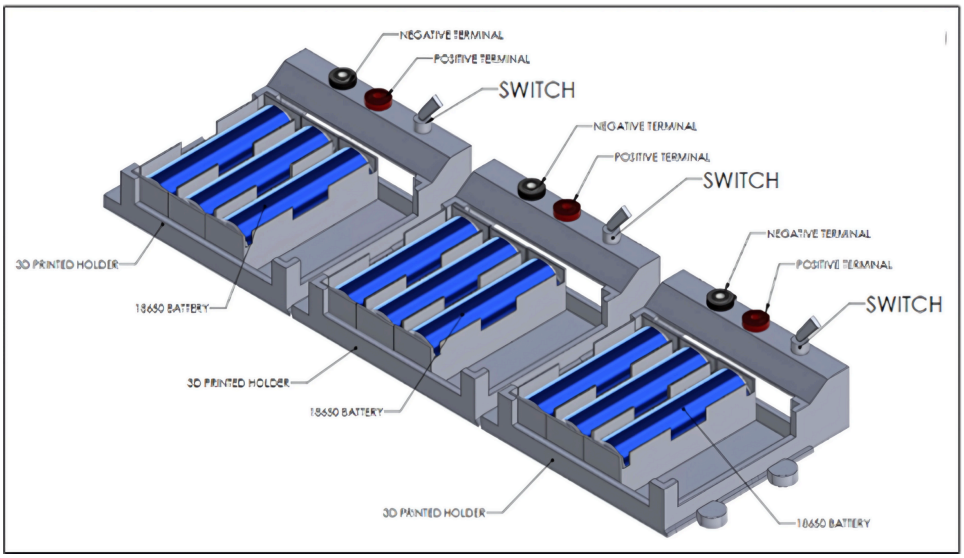

Fig. 3 3D rendering of the battery holders for the external discharging the 18650 batteries.

2.6 Statistical Analyses and Mathematical Modeling

After the discharging process, the residual voltage percent Et, percentage voltage drops Er, and discharge rate Ed are computed for each trial and is recorded in the response columns of the factorial table generated by the Design-Expert® software using CCD. Statistics analyses (i.e., Sequential Model of Sums, Lack of Fit Test, R squared, ANOVA) available in the software were utilized to understand the behavior of the variables—both input and response. The Design-Expert® software will also provide the optimized mathematical model (coded and actual equations), for RSM, in the form:

$$\hat{y}_n = \beta_0 + \beta_A A + \beta_B B + \beta_C B + \cdots + \beta_k k + \beta_{AB} AB +$$

$$\beta_{AC} AC + \cdots + \beta_{k(k-1)}(k-1)(k) + \beta_{AA} A^2 + \beta_{BB} B^2 + \cdots + \beta_{kk} k^2 \quad (1)$$

Where:
$\hat{y}_n$ is the response variable (R_1, R_2, R_3, …, R_n)
A, B, C …, k are the factors (independent) variables
β are the coefficients to be estimated by the model (e.g., linear and quadratic terms)

2.7 Model validation through optimization studies using the desirability function in Design-Expert®

One feature of the Design-Expert software is its capacity to produce desirability functions. The desirability function in Design-Expert software was implemented in this study as part of the optimization process to balance multiple response variables. The principles of Response Surface Methodology (RSM) and Central Composite Design (CCD) were followed. The desirability function allowed each response—Percent Voltage Drop (Er), Residual Voltage Percent (Et), and Discharge Rate (Ed)—to be transformed into a normalized scale ranging from 0 (undesirable) to 1 (highly desirable).

Specific optimization goals were assigned to each response variable, such as maximization, minimization, or targeting a specific range, and these goals were converted into individual desirability scores. The scores were then aggregated into a composite desirability function, enabling the simultaneous evaluation of all responses. This approach facilitated determining optimal conditions for the independent variables by maximizing the composite desirability score.

Implementing the desirability function ensured that trade-offs between competing responses were accounted for, allowing a systematic design of space exploration. This provided a robust framework for multi-objective optimization.

3 RESULTS AND DISCUSSIONS

This section presents the results of the optimization study on the discharging process of lithium-ion batteries (LIBs) using zinc powder as a catalyst, as analyzed through Response Surface Methodology (RSM). The experimental data were obtained using a Central Composite Design (CCD) and were evaluated to determine the influence of independent variables—NaCl concentration, discharging time, and zinc powder in NaCl solution—on key response variables: Percent Voltage Drop (Er), Residual Voltage (Et), and Discharge Rate (Ed). Statistical analyses, including ANOVA and model diagnostics, were employed to assess the significance of the factors and their interactions. The findings provide insights into the relationships between variables, enabling the development of predictive models for process optimization and laying the groundwork for efficient LIB recycling.

3.1 Factor Set-up and DoE from Design-Expert using Central Composite Design

A summary of the factor set-up and coded values is presented in Table 3 reports on the factor set-up and coded values for the Central Composite Design (CCD) used in the study. It defines three independent variables critical to optimizing the discharging process of lithium-ion batteries: NaCl concentration (A), discharging time (B), and zinc in NaCl solution (C). Each factor is expressed with its corresponding units, minimum and maximum values, coded low (-1), coded high (+1), and the mean value. NaCl concentration (A) varies between 9.27 wt.% and 22.73 wt.%, with a coded low value of 12 wt.% and a coded high value of 20 wt.%, and a mean value of 16 wt.%. This range captures the effect of electrolyte concentration on discharging efficiency. On the other hand, discharging time (B) ranges from 49.77 minutes to 100.23 minutes, with coded values set at 60 minutes (-1) and 90 minutes (+1) and a mean of 75 minutes. This range ensures the capture of time-dependent effects on voltage drop and discharge performance. And finally, Zinc in NaCl solution (C) is tested within 0.39 wt.% to 2.41 wt.%, with coded values of 0.80 wt.% (-1) and 2.00 wt.% (+1) and a mean of 1.40 wt.%. This variable evaluates the catalytic influence of zinc on the discharging process.

The factor set-up and coded values for CCD are essential because they ensure that the design space comprehensively explores the variables' linear, quadratic, and interaction effects, enabling efficient optimization of the discharging system [48].

For NaCl concentration, a coded high value is set at 20% as [33] showed that no significant changes in the discharging activity were observed beyond this electrolyte concentration. A coded low value of 12% is also chosen since it was also shown that this concentration reflects an effective LIB discharging because of the sufficient ionic strength that enhances the discharging activity [49]-[50]. Further, a coded low value of 60 mins and a coded high value of 90 minutes are set for the input variable time as this is also reflected that an efficient discharging happens at this range, including the 75 mins as the center point.

Regarding the range for the S/L Ratio, the high value of 2% and low value of 0.8% are set for the benchmarking experiments. As shown in the behavior of different S/L ratios in Fig. 4, there are no significant differences in the percent residual voltage, and the 2% S/L ratio showed a high discharge rate in the first 30 minutes, which is preferable as it could minimize the time needed to fully discharge an LIB [51]-[53]. Moreover, agitation as a categorical variable in the study was not included, as it shows in Fig. 5 that there is no significant difference in the percent residual voltage. In fact, the experimental run with a 1% S/L ratio (not stirred) performed the best out of the trials.

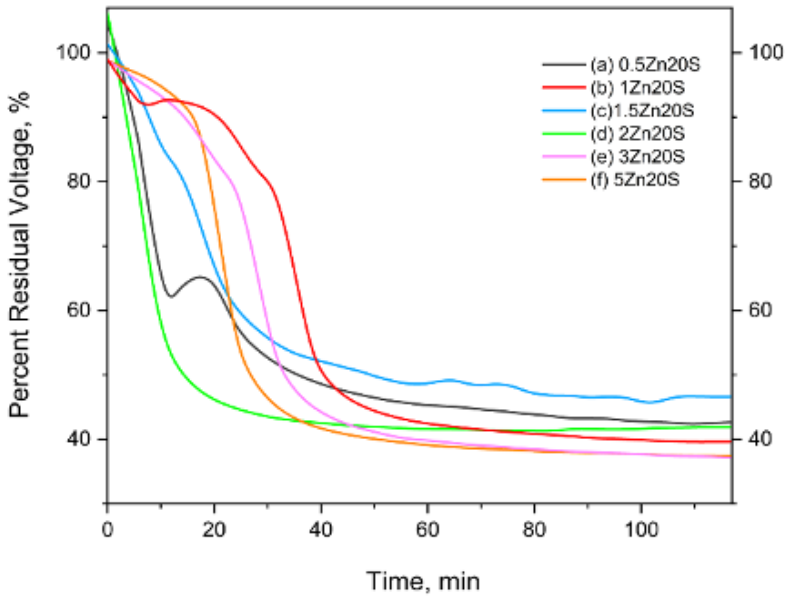

Fig. 4. Discharging behavior of benchmark experiments on Zn-NaCl S/L ratio with no stirring using 20% NaCl concentration: (a) 0.5%; (b) 1.0%; (c) 1.5%; (d) 2.0%; (e) 3.0%; (f) 5.0%.

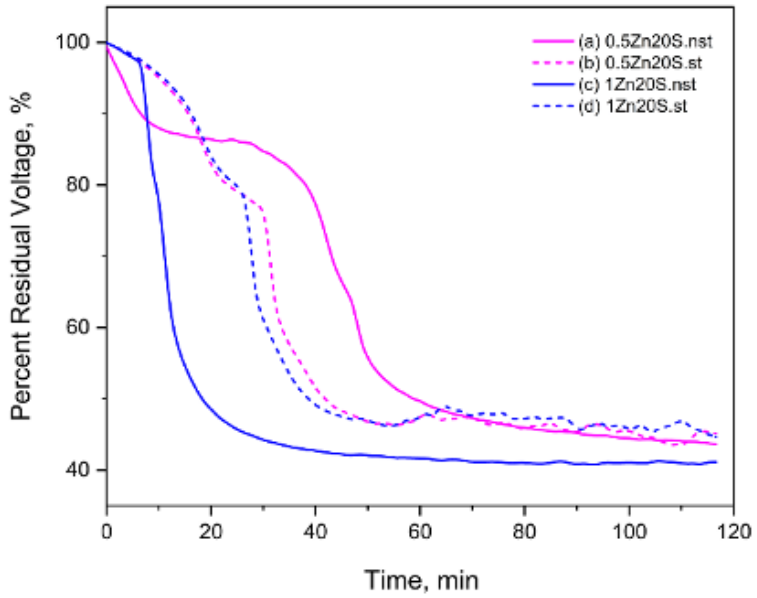

Fig. 5. Discharging behavior of benchmark experiments on inclusion of categorical variable on agitating the slurry at 20% NaCl concentration: (a) 0.5% S/L ratio (no stirring); (b) 0.5% S/L ratio (with stirring); (c) 1.0% S/L ratio (no stirring); (d) 1.0% S/L ratio (with stirring).

Table 3. Factor Setup and Coded values for CCD.

Factor	Name	Units	Min	Max	Coded Low	Coded High	Mean
A	[NaCl]	wt.%	9.27	22.73	-1 ↔ 12.00	+1 ↔ 20.00	16.00
B	Time	mins	49.77	100.23	-1 ↔ 60.00	+1 ↔ 90.00	75.00
C	Zn-NaCl Solution Ration	wt.%	0.3909	2.41	-1 ↔ 0.80	+1 ↔ 2.00	1.40

Upon confirming the coded values for all the input variables, the software generated a DoE containing 19 runs. The generated DoE shown in Table 4 is systematically structured to explore the design space comprehensively and efficiently. Randomization was incorporated into the design, as evidenced by the differing standard (Std.) and run orders, to mitigate systematic biases and ensure the reliability of results. Replicated center points were included, such as in Runs 2, 4, 8, 12, and 17, to assess the experimental error and improve the statistical robustness of the analysis. These center points also enhance the precision of the model, providing a solid foundation for estimating curvature and validating the reproducibility of the experimental setup.

Table 4. Factor Setup and Coded values for CCD.

Std.	Run	A: NaCl, %	B: Time, mins	C: S/L Ratio, %
11	1	16.00	49.77	1.40
15	2	16.00	75.00	1.40
5	3	12.00	60.00	2.00
19	4	16.00	75.00	1.40
12	5	16.00	100.23	1.40
14	6	16.00	75.00	2.41
9	7	9.27	75.00	1.40
16	8	16.00	75.00	1.40
10	9	22.73	75.00	1.40
6	10	20.00	60.00	2.00
7	11	12.00	90.00	2.00
18	12	16.00	75.00	1.40
1	13	12.00	60.00	0.80
13	14	16.00	75.00	0.39
8	15	20.00	90.00	2.00
4	16	20.00	90.00	0.80
17	17	16.00	75.00	1.40
3	18	12.00	90.00	0.80
2	19	20.00	60.00	0.80

3.2 Electrochemistry of the Discharging Process using NaCl electrolyte with Zn Powder Catalyst

Studies [54]-[56] have shown that during the discharge of lithium-ion batteries (LIBs), when the anode and cathode interact with a salt-containing electrolyte (e.g., NaCl), electrochemical reactions occur within the electrolyte circuit. The battery's voltage drop is attributed to the water electrolysis process, where water molecules are split into hydrogen (H_2) and oxygen (O_2) gases. In the external discharging of 18650 lithium-ion batteries in an aqueous NaCl solution, incorporating zinc powder significantly influences the electrochemical processes and enhances the efficiency of energy neutralization. This setup, involving SS316L electrodes submerged in a slurry of NaCl electrolyte with zinc powder, facilitates controlled redox reactions at the electrodes while taking advantage of the catalytic activity of zinc to optimize the discharging process. The interaction of these factors not only accelerates the reactions but also provides insights into the implications for material durability and process sustainability.

3.2.1 Reaction at the cathode

At the cathode, reduction reactions dominate, with the primary reaction involving the reduction of water molecules:

$$2\ H_2O + 2e^- \rightarrow H_2 + 2\ OH^- \quad E° = 0.00\ V \quad (2)$$

This reaction results in the formation of hydrogen gas (H2), observed as bubbles at the electrode surface, and hydroxide ions (OH-), which increase local alkalinity. The availability of electrons from the external circuit drives this reaction, making it the primary driver of gas evolution at the cathode.

In the presence of dissolved zinc ions (Zn2+) another significant reduction reaction occurs:

$$Zn^{2+} + 2e^- \rightarrow Zn \quad E° = -0.76\ V \quad (3)$$

Here, zinc ions are reduced back to metallic zinc, which may deposit near the cathode or disperse in the electrolyte. This reaction provides an additional pathway for electron consumption, enhancing overall discharge efficiency. The reduction of zinc ions competes with the reduction of water, depending on local concentrations and electrode potential.

3.2.2 Reaction at the Anodes

Oxidation reactions at the anode are equally crucial in the discharge process. Water and chloride ions participate in these reactions, depending on the conditions:

$$H_2O \rightarrow \tfrac{1}{2}\,O_2 + 2\,H^+ + 2e^- \quad E° = +1.23\ V \quad (4)$$

This reaction results in the production of oxygen gas (O2) and protons (H+), which decrease the local pH near the anode. The evolution of oxygen gas is typically observed in less concentrated chloride environments.

In high chloride environments, chloride oxidation becomes favorable:

$$2\,Cl^- \rightarrow Cl_2 + 2e^- \quad E° = +1.36\ V \quad (5)$$

This reaction produces chlorine gas (Cl2), a toxic byproduct. Although this reaction is less thermodynamically favorable than oxygen evolution, it often dominates due to the high chloride ion concentration in NaCl solutions. The prominence of this reaction highlights the aggressive nature of the electrolyte at the anode. Simultaneously, the zinc powder in the electrolyte undergoes oxidation:

$$Zn \rightarrow Zn^{2+} + 2e^- \quad E° = +0.76\ V \quad (6)$$

This reaction contributes electrons to the circuit, increasing the electron flow and facilitating other oxidation reactions. The cycling of zinc between its ionic and metallic states stabilizes the redox environment, improving the overall discharge efficiency.

3.2.3 Electrolyte Dynamics

The NaCl solution acts as a medium for ion transport and a source of reactive species. The dissociation of NaCl:

$$NaCl \rightarrow Na^+ + Cl^- \quad (7)$$

provides chloride ions (Cl- for oxidation at the anode and sodium ions (Na+) for charge neutrality. The ionic conductivity of the NaCl solution ensures efficient electron flow between the electrodes, reducing resistance in the system. The addition of zinc powder increases the ionic strength of the solution through the dissolution of zinc ions (Zn2+). However, the formation of zinc hydroxide (Zn(OH)2) in alkaline conditions near the cathode can limit the long-term stability of the electrolyte. Zinc facilitates faster reaction rates by acting as a redox mediator, reducing overpotentials for water electrolysis and chloride oxidation, which leads to increased gas evolution rates, especially in the early stages of discharging. The reversible cycling of zinc between its metallic and ionic states stabilizes the electrolyte, mitigating localized charge imbalances and improving the consistency and uniformity of the discharge process. At the anode, zinc oxidation competes with chloride and water oxidation, partially protecting the SS316L electrode from aggressive chloride attack, although pitting corrosion remains a concern due to high chloride concentrations. Overall, the presence of zinc enhances the system's discharge efficiency by providing additional redox pathways, ensuring that the battery's stored energy is neutralized more effectively and reducing the time required for complete discharge. However, zinc's catalytic activity amplifies the production of hydrogen and chlorine gases, necessitating proper gas management systems to handle these byproducts safely and

prevent hazardous accumulation. Nevertheless, it is essential to note that the possibility of chlorine gas formation at the anode is limited by ion transport and diffusion factors, particularly at lower salt concentrations.

3.3 Voltage Profiles following the Experimental Runs of the DoE

A summary of the initial voltage (V0) and final voltage (Vt) is shown in table 5 with 19 generated runs by the software using CCD. As the design of the discharging jig suggests, three batteries can be simultaneously discharged and are considered the triplicates per experimental run of the DoE, labeled E1, E2, and E3 representing each of the discharging slots.

Table 5. Average V0 and Vt for each of the DoE generated experimental run with coded values of the factors.

	Factor Actual Values			Factor Coded Values			Voltage Profile	
Run	NaCl, %	Time, mins	S/L Ratio, %	NaCl (A)	Time (B)	S/L Ratio (C)	V_0, Vave	Vt, Vave
1	16.00	49.77	1.40	0.0	-1.68	0.0	3.497	1.629
2	16.00	75.00	1.40	0.0	0.0	0.0	3.535	1.551
3	12.00	60.00	2.00	-1.0	-1.0	1.0	3.591	1.665
4	16.00	75.00	1.40	0.0	0.0	0.0	3.627	1.58
5	16.00	100.23	1.40	0.0	1.68	0.0	3.392	1.384
6	16.00	75.00	2.41	0.0	0.0	1.68	3.521	1.587
7	9.27	75.00	1.40	-1.68	0.0	0.0	3.525	1.528
8	16.00	75.00	1.40	0.0	0.0	0.0	3.567	1.451
9	22.73	75.00	1.40	1.68	0.0	0.0	3.454	1.437
10	20.00	60.00	2.00	1.0	-1.0	1.0	3.494	1.64
11	12.00	90.00	2.00	-1.0	1.0	1.0	3.512	1.604
12	16.00	75.00	1.40	0.0	0.0	0.0	3.591	1.6035
13	12.00	60.00	0.80	-1.0	-1.0	-1.0	3.642	1.729
14	16.00	75.00	0.39	0.0	0.0	-1.68	3.572	1.544
15	20.00	90.00	2.00	1.0	1.0	1.0	3.433	1.503
16	20.00	90.00	0.80	-1.0	0.0	-1.0	3.561	1.633
17	16.00	75.00	1.40	1.0	1.0	-1.0	3.512	1.451
18	12.00	90.00	0.80	-1.0	1.0	-1.0	3.646	1.703
19	20.00	60.00	0.80	1.0	-1.0	-1.0	3.507	1.676

Still in Table 5, an average of the initial voltage V0 and final voltage Vt after time t in minutes es assigned for each of the discharging runs according to the DoE. This approach enables a more accurate and comprehensive reflection of the discharge behavior across various experimental conditions. By meticulously assigning and monitoring each experimental run, this technique ensures that the resulting data is both reliable and representative. Consequently, it allows for the discernment of subtle variations and patterns in discharge behavior, thereby enhancing the overall robustness and validity of the study's findings.

It can also be observed in Table 5 that the final voltage for all the experimental runs is well below 2.5 V, which is a threshold that is required to process 18650 batteries for recycling. These values for the final voltage are also below the safe state of charge (SOC), which is 40%-60% of the 18650 batteries' full capacity at ~3.7V. For batteries below the safe SOC, further processing, such as recycling, is preferred because these batteries are less likely to pose risks like thermal runaway or fire hazards during handling [57]-[58]. It can further be observed that residual voltage is still present ~1.4V to ~1.7V, and no further discharging happens, despite the different conditions for the independent variables for each of the experimental runs. This can be attributed to the fact that some secondary batteries (e.g., 18650-type) have cut-off voltage and discharge protection circuits.

Cutoff voltage is defined as the voltage of a battery wherein no further discharging happens (considered fully discharged) to prevent it from entering a deep discharge state (over-discharging) which could cause internal short circuit and capacity degradation [59]. Deep discharge can be avoided using discharge protection circuits in the battery, which can be present in LIBs such as 18650 batteries. Pushing the discharge below the cutoff voltage could lead to deep discharge, which is not ideal for batteries intended for recycling. When a battery is deeply discharged, the residual lithium can become more difficult to extract efficiently. This is because the electrochemical processes used in recycling, such as electrochemical leaching and electrodeposition, are less effective at recovering lithium from batteries that are not within an optimal voltage range[60]-[64].

Another explanation for the terminated discharging avoiding complete voltage depletion and the presence of residual voltage for each run is the nature of the discharging setup. The study was externally discharging the battery, meaning no direct contact on the batteries' electrodes to the zinc-catalyzed NaCl electrolyte. The external discharging method was used because the battery electrodes could corrode when in contact with the NaCl electrolyte, as studied by R. Farzana, R. Rajarao, P. Ranjan Behera, K. Hassan, and V. Sahajwalla [65]. This is also not an ideal condition as it could damage the electrode materials, making it more difficult to recover valuable metals like lithium and cobalt during the recycling process. Furthermore, corrosion can lead to solid residues and by-products forming, which can complicate the recycling process and require additional steps to manage [66].

In this study, the external discharging method terminates the discharge process when the current approaches zero, signifying that the battery has expended most of its energy. As the battery discharges, its voltage steadily declines. When the voltage drops to a certain level, the current diminishes and eventually reaches ~0.0V. This occurs because the battery can no longer sustain a sufficient potential difference to drive the current through the circuit. Consequently, the discharge process naturally stops, leaving behind a residual voltage. This behavior is illustrated in Fig. 6. The graph illustrates a steady decrease in current over time, eventually reaching a point where it approaches zero. At this stage, the voltage stabilizes at a residual level, indicating that the discharge process has ceased. This discharging method effectively prevents over-discharge, thereby mitigating risks such as thermal runaway or internal damage to the battery. Similar observations have been reported in other studies utilizing external discharging methods. These methods halt the discharging process at low current levels, ensuring that the state of charge (SOC) remains within safe limits, which is crucial for safe recycling practices [67].

The Design of Experiments (DoE) generated by the software was meticulously followed and implemented, ensuring that the relationships and mathematical models were accurately represented. The voltage profiles obtained from different experimental runs demonstrated varied behaviors corresponding to the differing experimental conditions. These profiles provide valuable insights into the relationships between the variables under study.

Notably, some replicates and runs exhibited noise and fluctuations, which are indicative of the inherent variability in the experimental setup and conditions. These variations will be discussed in detail in subsequent sections to better understand their impact and to refine the experimental approach further.

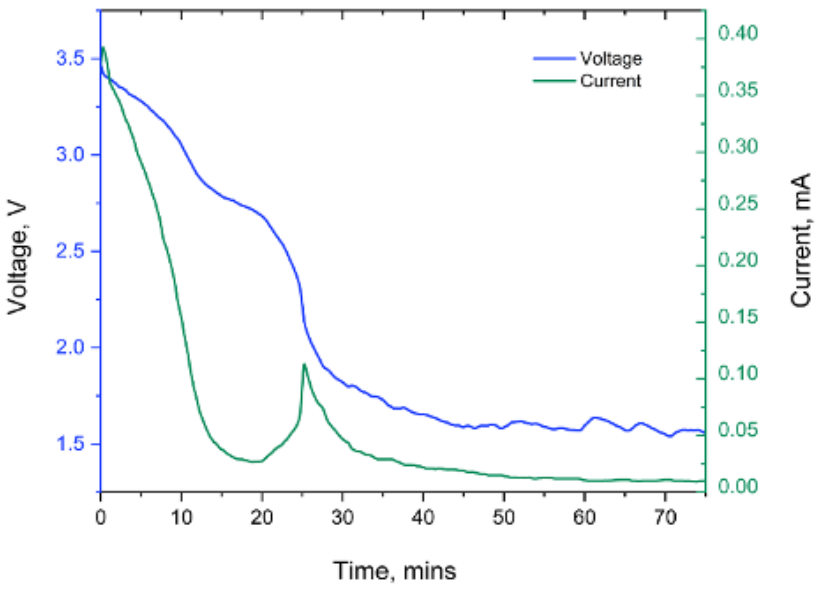

Fig. 6. Voltage and Current behavior for the discharging of Run 4 (center point) of the DoE.

3.3.1 Voltage profiles of runs with center points

Fig. 7 shows the runs with similar values for each input variable which are the median coded values (typically coded as 0) for all factors, referred to as center points. Center points are experimental runs where each input variable is set to its median or middle value, typically coded as 0 in the design matrix. For example, within a coded range of -1 to +1, the center point is represented by 0 for each variable. Center points are integral to experimental designs like those used in Central Composite Designs (CCD) in this study. Their primary function is to estimate pure error by replicating runs at identical settings, thereby enhancing the precision of statistical analysis and error estimation. Additionally, center points are pivotal in detecting non-linearity in the response surface, providing critical insights into whether a quadratic model more accurately describes the system's behavior. These designs achieve improved balance, robustness, and reliability by incorporating replicated center points, ultimately strengthening the overall model [68].

The voltage profiles from the experimental runs provide critical insights into the discharging behavior of LIBs within a system optimized through RSM using a Central Composite Design (CCD). Each profile illustrates the changes in residual voltage over time under varying experimental conditions, where the independent variables include NaCl concentration, discharging time, and Zn powder concentration. These patterns are instrumental in understanding the dynamics of the discharging process, thereby facilitating the development of a robust optimization model for safe and efficient battery recycling.

The voltage profiles obtained from the experimental runs in Fig. 7 (A, run 2; B, run 4; C, run 8; and D, run 17), despite identical conditions for NaCl concentration, discharging time, and Zn-NaCl solution ratio, reveal variations in the behavior of residual voltage over time. These differences, though subtle, provide information into the underlying electrochemical dynamics and potential factors influencing the discharging process. Each voltage profile generally exhibits a sharp initial drop, followed by gradual stabilization near ~1.5 V. This pattern reflects the discharging process of lithium-ion batteries, where the rapid initial voltage decline corresponds to high reaction rates driven by the battery's starting voltage (~3.7 V) [69].

The stabilization phase indicates the battery approaching a fully discharged state, where residual voltage is minimized. While this trend is consistent, differences in the voltage drop's steepness, stabilization timing, and fluctuations during the discharge process suggest additional influences at play[70]. The variability in voltage profiles, despite identical conditions for NaCl concentration, discharging time, and Zn-NaCl solution ratio, can be attributed to several factors: (1) Electrode Surface Inconsistencies, where SS316L electrodes used in the study may exhibit surface inconsistencies such as micro-corrosion, uneven passive layer formation,

or differences in the surface area exposed to the electrolyte which alter local current density and reaction rates, affecting the voltage profile; (2) Electrical Connection Variability, where minor inconsistencies in the electrical connection between the electrodes and the battery terminals may introduce variability in the overall circuit resistance, leading to slight differences in the rate of voltage drop across runs [71]; (3) Zinc Powder Distribution, where the distribution of zinc powder within the electrolyte can vary even though S/L ratio of the slurry is constant. Uneven dispersion or agglomeration of zinc particles can lead to localized variations in catalytic activity, resulting in differing reaction kinetics across the material. This non-uniform distribution can cause certain areas to exhibit higher or lower catalytic efficiency, impacting the overall performance and consistency of the reaction process [72]. Runs with better zinc dispersion may exhibit faster initial voltage drops due to enhanced electron transfer rates, whereas runs with agglomerated zinc might show slower discharge behavior; (4) Localized Ionic Strength and pH Changes: Despite identical NaCl concentrations, localized changes in ionic strength and pH near the electrodes can influence the voltage profiles. For instance, the reduction of water at the cathode produces hydroxide ions, increasing local alkalinity and potentially leading to the formation of zinc hydroxide ($Zn(OH)_2$). This precipitation can temporarily impede reaction kinetics, introducing fluctuations in the voltage profile. Similarly, the evolution of gases (hydrogen at the cathode and oxygen or chlorine at the anode) may alter local electrolyte dynamics, further contributing to variability; and (5) Battery Internal Differences: Even among batteries of the same type, slight differences in internal resistance, state of charge, or manufacturing tolerances can influence discharging behavior [73]-[74]. A battery with higher internal resistance or a partially degraded cell may exhibit a slower voltage decline compared to a newer or less degraded battery under identical conditions [75].

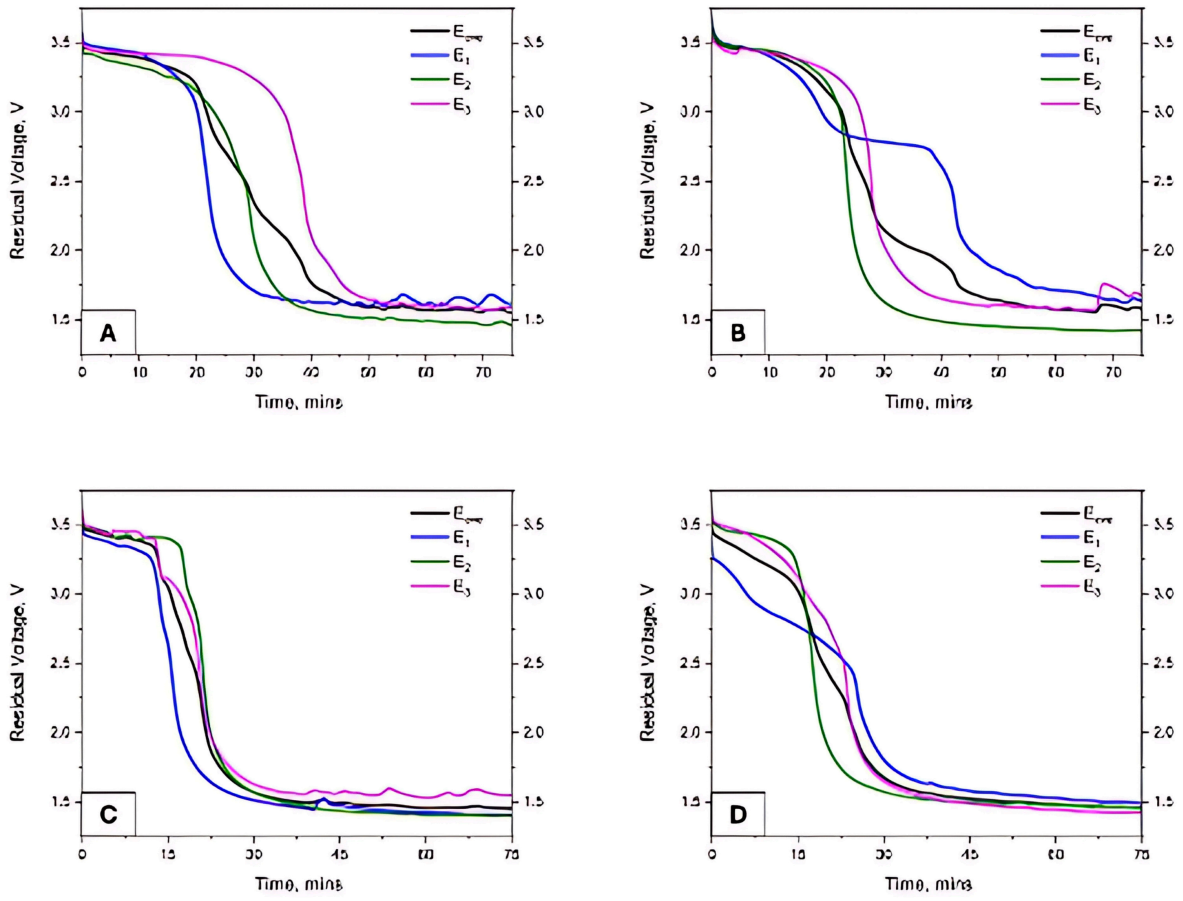

Fig. 7. Voltage profiles of experimental runs in DoE with center points: (A) Run 2; (B) Run 4; (C) Run 8; and (D) Run 17.

Voltage profile variability highlights replicates' critical role in experimental designs. These replicates are essential for capturing the system's natural variability, allowing for accurate estimation of pure error and detecting subtle trends that might otherwise remain hidden. By addressing sources of variability, such as improving electrode consistency and ensuring uniform zinc dispersion, the reproducibility and reliability of experimental results are significantly enhanced. Importantly, all replicates in runs 2, 4, 8, and 17 consistently remained below the safe state of charge (SOC) of approximately 2.5 V and did not exceed the preferred cutoff voltage range of 1.4 V to 1.7 V for 18650 batteries. This consistency is a strong indicator of the effectiveness of the discharging process and is particularly advantageous for recycling, ensuring that the batteries are safely discharged and optimally prepared for processing. These results affirm the robustness of the methodology and its potential for reliable application in battery recycling.

3.3.2 Effect of NaCl Concentration

A comparison of the voltage profile and discharge behavior on the axial points (± α; run 7 and run 9) of input variable A (NaCl concentration and the center points (runs 8 and 17) is shown in Fig. 7. Fig. 8A (Run 7, -α), representing the lowest level of NaCl concentration, has demonstrated a slow and gradual decline in voltage. This behavior indicates that a lower ionic strength in the electrolyte reduces the system's ability to transport ions efficiently, which in turn slows the electrochemical reactions responsible for discharging [76]-[78].

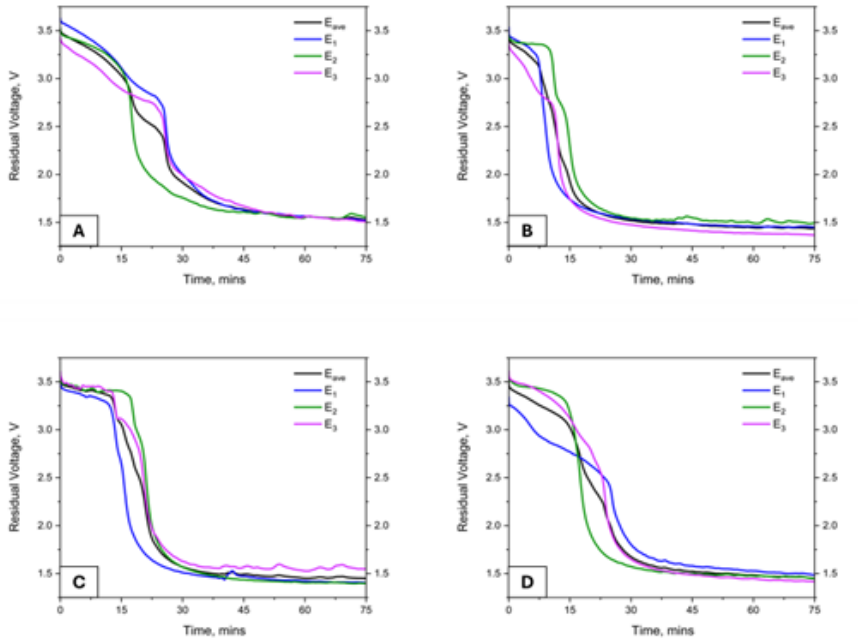

Fig. 8. Voltage profiles of experimental runs to compare the effect NaCl concentration evaluating the runs with axial points on A) run 7 (Factor A= -α) and B) run 9 (Factor A= +α) and the center point for C) run 8 and D) run 17 (Factor A=0; Factor B=0; Factor C=0)

As a result, the voltage has stabilized at a later stage of the discharge process, signaling inefficiency in neutralizing the battery's residual energy. This highlights the challenges posed by low NaCl concentrations in achieving rapid and complete discharge. In contrast, Fig. 9B (run 9, +α), corresponding to the highest level of NaCl concentration, has exhibited a steeper initial decline in voltage and an earlier stabilization phase. This profile reflects the enhanced ionic conductivity provided by a high NaCl concentration, which facilitates faster electron transfer and accelerates the reaction kinetics [79]. The efficiency of this run underscores the importance of optimizing electrolyte composition to ensure effective energy neutralization. The stark differences between the voltage profiles of Figs. 8A and 8B (runs 7 and 9) have illustrated the critical role of NaCl concentration in influencing the discharging process.

The profiles for Figs. 8C and 8D (runs 8 and 17), which have represented center points (A=0, B=0, C=0), have provided an intermediate perspective. The initial decline in voltage has been faster than in Fig. 8A (run 7) but slower than in Fig. 8B (run 9), reflecting the balanced ionic strength of the electrolyte at median NaCl levels. Both runs have exhibited consistent stabilization phases, highlighting the reproducibility of the system under these conditions. The behavior observed in Figs. 8C and 8D (runs 8 and 17) has served as a baseline for understanding the average performance of the discharging process and offers a reliable benchmark for assessing variability across the design.

When comparing the extreme Fig. 8A (run 7) and Fig. 8B (run 9), to the center points Figs. 8C and 9D (runs 8 and 17), more information can be deduced. The efficiency of discharge has improved significantly with higher NaCl concentrations, as demonstrated by the rapid voltage decline and earlier stabilization in Fig. 8B (run 9). Conversely, the slower voltage decline in Fig. 8A (run 7) has highlighted the inefficiency of lower ionic strengths. Meanwhile, the center points have exhibited moderate behavior, suggesting a balanced impact of NaCl concentration, time, and Zn powder concentration. The consistency between Figs. 8C and 8D (runs 8 and 17) further confirms the robustness of the experimental set-up and highlights the stability of the system under average conditions.

These observations have important implications for the study's objectives. First, the inclusion of extreme and center-point runs in the design validates the experimental approach, ensuring that the RSM-CCD captures both linear and non-linear effects of NaCl concentration. Second, the profiles reveal a clear relationship between NaCl concentration and discharging behavior, with runs at higher concentrations significantly enhancing the process efficiency. Finally, the voltage profiles provide critical data for developing a mathematical model to predict response variables such as Percent Voltage Drop (Er), Residual Voltage (Et), and Discharge Rate (Ed). For instance, the steep declines in Fig. 8B (run 9) and Fig. 8C (run 8) correspond to higher Er and Ed, while the delayed stabilization in Fig. 8A (run 7) reflects a higher Et.

3.3.3 *Effect of Time*

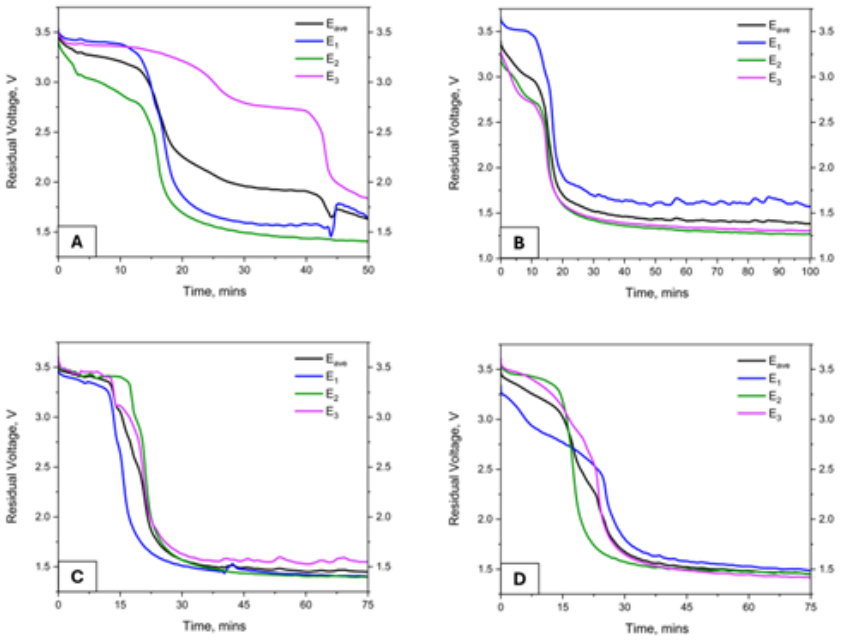

Fig. 9. Voltage profiles of experimental runs to compare the effect time evaluating the runs with axial points on A) run 1 (Factor B= -α) and B) run 5 (Factor B= +α) and the center point for C) run 8 and D) run 17 (Factor A=0; Factor B=0; Factor C=0)

The graph profiles another input variable B (time) and provides an important report on its effect in the discharging of LIBs. Fig. 9A presents run 1, with the shortest discharging time (-α), Fig. 9B (run 5), with the longest discharging time (+α), and Figs. 9C and 9D (runs 8 and 17), serving as center points (Factor B=0), were fundamental for this investigation. A rapid initial voltage decline was observed, followed by stabilization at a relatively high residual voltage exhibited by Fig. 9B (run 5). This early voltage drop indicates an efficient start to the discharge process. However, the limited duration highlights areas for improvement in fully neutralizing the residual energy. This insight is valuable for enhancing battery preparation methods for recycling. The results from Fig. 9B (run 5) underline the potential for optimizing discharging durations to achieve better outcomes. Conversely, Fig. 9A (run 1) demonstrated a gradual voltage decline, ultimately stabilizing at a much lower residual voltage. The extended discharging time facilitated a more thorough process, ensuring most of the residual energy was neutralized. This emphasizes the benefits of longer discharging durations, highlighting their role in achieving complete energy dissipation and safe battery recycling. The results from Fig. 9B (run 5) emphasize the efficiency and effectiveness of extended discharging times in meeting the study's objectives [80].

Figs. 8C and 8D (runs 8 and 17), which served as the center points for all variables, exhibited intermediate behavior compared to Figs. 9A and Fig. 9B (runs 1 and 5), respectively. The initial voltage decline in these runs was faster than in Fig. 9A (run 1) but slower than in Fig. 8B (run 5), with stabilization occurring at a moderate residual voltage. The consistency of these profiles underscores the robustness and reproducibility of the experimental design, offering a balanced perspective on the discharging process under median conditions. These center-point runs serve as benchmarks for understanding average system performance, reinforcing the study's reliability. When comparing the axial points—Figs. 8A and Fig. 8B (runs 1 and 5)—to the center points, Figs. 9C and 9D (runs 8 and 17), the critical influence of discharging time on the process becomes evident. Fig. 9B (run 5), with the longest duration, achieved the lowest residual voltage, ensuring the most complete discharge. In contrast, Fig. 9A (run 1) stabilized at a higher residual voltage, demonstrating the need for optimizing shorter discharging times. The center-point runs, meanwhile, provides a reliable baseline for evaluating system behavior, balancing efficiency and completeness. The consistency between Figs. 9C and 9D (runs 8 and 17) further validates the experimental setup's robustness.

The distinct behaviors across the runs confirm the appropriateness of the RSM-CCD design, which systematically explores the effects of extreme and median values of discharging time. By capturing these variations, the design enables a comprehensive analysis of time as an independent variable. The comparison also highlights the relationship between discharging time and efficiency, with longer times facilitating more complete energy dissipation and shorter times presenting opportunities for optimization [68].

Additionally, the voltage profiles provide critical data for formulating a predictive model for response variables such as Percent Voltage Drop (Er), Residual Voltage (Et), and Discharge Rate (Ed). Runs with longer discharging times, like Fig. 9B (run 5), exhibited higher Er and lower Et, reflecting their efficiency in completing the process. In contrast, shorter discharging times, as seen in Fig. 9A (run 1), resulted in lower $Er$and higher Et. The discharge rate (Ed) is evident in the slope of the initial voltage decline, with Fig. 9A (run 1) showing a rapid early discharge and Fig. 9B (run 5) demonstrating a steadier, extended discharge process.

3.3.4 Effect of Zinc-NaCl Solution Ratio (S/L Ratio)

The solid-to-liquid (S/L) ratio is one of the variables being studied on its possible impacts on the discharging efficiency of lithium-ion batteries (LIBs) through influencing catalytic activity and ionic mobility. This section examines the effects of varying S/L ratios, highlighting the differences between extreme and center-point conditions to better understand its role in optimizing the discharging process for recycling as shown in Fig. 10. Figs. 10A and 10B (runs 14 and 6) correspond to the lowest (C = -α) and highest (C = +α) coded levels of the S/L ratio, respectively, while Figs. 10C and 10D (runs 8 and 17) serve as center points (C = 0) for all variables. A comparative analysis of these profiles highlights the role of the S/L ratio in optimizing discharging efficiency and completeness.

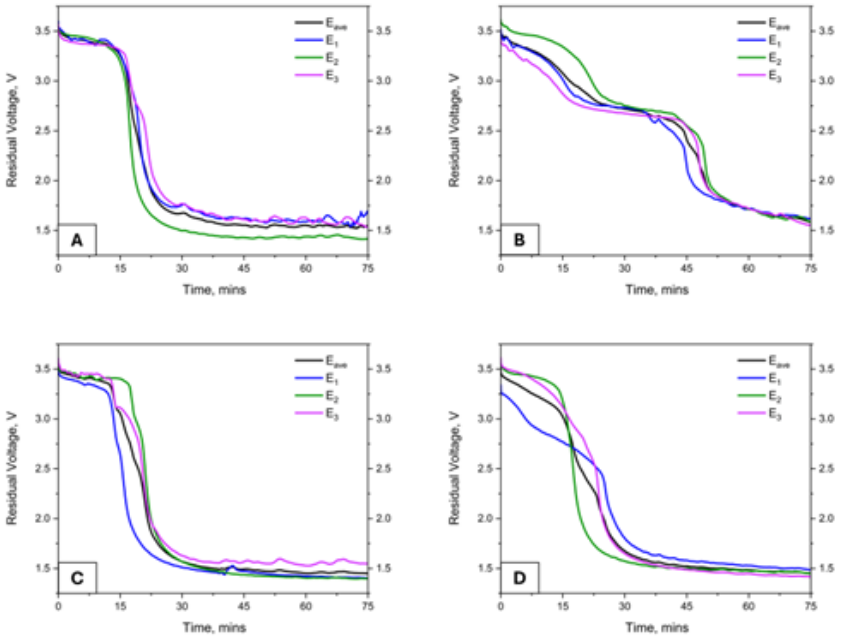

Fig. 10. Voltage profiles of experimental runs to compare the effect of S/L ratio evaluating the runs with axial points on A) run 14 (C= -α) and B) run 6 (C= +α) and the center point for C) run 8 and D) run 17 (Factor A=0; Factor B=0; Factor C=0)

Fig. 10A (run 14) exhibited a sharp initial voltage decline, indicating an effective start to the discharging process. However, the stabilization phase occurred earlier with a higher residual voltage, suggesting that the lower S/L ratio reduced the catalytic efficiency of the zinc powder. The limited catalytic activity at this ratio likely resulted in incomplete energy dissipation, leaving more residual energy in the battery. This behavior highlights the challenges posed by insufficient zinc powder levels in sustaining the discharging process for a complete reaction.

In contrast, Fig. 10B (run 6), corresponding to the highest coded level (C = +α), showed a more gradual voltage decline with a prolonged stabilization phase. The higher concentration of zinc powder enhanced catalytic activity, allowing the discharge process to continue over a longer period and achieve a lower residual voltage. However, the slower initial voltage decline may be attributed to potential drawbacks such as increased viscosity or agglomeration of zinc particles in the solution, which can create localized resistance and reduce ionic mobility. Despite these limitations, the extended stabilization phase demonstrated the ability of a high S/L ratio to facilitate a more complete discharge.

Figs. 10C and 10D (runs 8 and 17), representing the center points (C = 0), displayed intermediate behavior between the extremes of Figs. 10A and 10B (runs 14 and 6). The initial voltage decline was faster than in Fig. 10B (run 6) but slower than in Fig. 10A (run 14), while the stabilization phases occurred at similar residual voltages. These profiles suggest balanced catalytic efficiency and ionic mobility under median conditions. The consistency observed between Figs. 10C and 10D (runs 8 and 17) highlights the reproducibility of the experimental design and provides a reliable baseline for evaluating the effects of extreme S/L ratios.

A comparison of the behavior of the axial points with the center points reveals important trends. At the lowest S/L ratio, Fig. 10A (run 14) achieved a rapid discharge initiation but failed to sustain the reaction for complete energy dissipation. Conversely, in the highest S/L ratio, Fig. 10B (run 6) extended the discharge process for a more thorough reaction but started with a slower rate. The center points struck a balance between these extremes, achieving consistent and efficient discharge without significant limitations. This comparison underscores the critical role of the S/L ratio in determining the efficiency and completeness of the LIB discharging process.

The behavior of these runs has significant implications for the study's objectives. The profiles validate the effectiveness of the RSM-CCD design in capturing the effects of varying S/L ratios, with the inclusion of extreme and center-point runs providing comprehensive coverage of the experimental space. The observed trends confirm the importance of the S/L ratio as an independent variable and highlight the interplay between catalytic efficiency and ionic mobility in optimizing the discharging process.

Furthermore, these voltage profiles provide critical data for modeling response variables such as Percent Voltage Drop (Er), Residual Voltage (Et), and Discharge Rate (Ed). For instance, Figs. 10B and 10C (runs 6 and 8) exhibited higher Er, indicating greater discharging efficiency, while Fig. 10A (run 14) showed lower Er, reflecting less energy dissipation. Similarly, the stabilization phases at lower residual voltages in Figs. 10B and 10C (runs 6 and 8) highlighted improved energy dissipation compared to the higher residual voltage in Fig. 10A (run 14). The initial slopes of the profiles also revealed faster discharge rates in Fig. 10A (run 14), while Figs. 10C and 10D (runs 8 and 17) represented moderate rates, providing a balanced perspective on the discharging process.

Table 6. Summary of the generated DoE with the corresponding values of the responses

	Factor 1	Factor 2	Factor 3	Response 1	Response 2	Response 3
Run	A: NaCl wt.%	B: Time mins	C: S/L Ratio wt.%	Voltage Drop %	Residual Voltage %	Discharge Rate V/min
1	16	49.77	1.4	53.42	46.58	0.038
2	16	75	1.4	56.12	43.88	0.026
3	12	60	2	53.63	46.37	0.032
4	16	75	1.4	56.44	43.56	0.027
5	16	100.23	1.4	59.2	40.8	0.02
6	16	75	2.42	54.93	45.07	0.026
7	9.27	75	1.4	56.65	43.35	0.027
8	16	75	1.4	59.32	40.68	0.028
9	22.73	75	1.4	58.4	41.6	0.027
10	20	60	2	53.06	46.94	0.031
11	12	90	2	54.33	45.67	0.021
12	16	75	1.4	55.35	44.65	0.027
13	12	60	0.8	52.53	47.47	0.032
14	16	75	0.39	56.77	43.23	0.027
15	20	90	2	56.22	43.78	0.021
16	20	90	0.8	54.14	45.86	0.021
17	16	75	1.4	58.68	41.32	0.027
18	12	90	0.8	53.29	46.71	0.022
19	20	60	0.8	52.21	47.79	0.031

This uniformity, even under varying conditions, highlights the reliability and safety of the discharging process, ensuring that the batteries are discharged to a level suitable for recycling. The consistent residual voltages across triplicates also underscore the robustness of the methodology, demonstrating its capacity to deliver repeatable and effective results in preparing LIBs for safe and optimal recycling. These findings reinforce the potential of this approach for practical applications in battery recycling processes.

3.4 Input-Response Variable Relationships and Statistical Model Analyses

In addition to examining the influence of the input variables on the voltage profile during the discharging process of LIBs for battery recycling, the study aimed to clarify the interactions and relationships between the input variables: (A) NaCl concentration; (B) time; and (C) zinc-NaCl solution ratio (SL ratio), and the response variables: (1) percent voltage drop (Er); (2) residual voltage percent (Et); and (3) discharge rate (Ed). These interactions were further quantified through statistical analysis of the models generated based on the response variable values obtained from each experimental run.

For each of the experimental run, the response variables are calculated as follows [34]:

(1)Percent Voltage Drop (in %), Er

Signifies the percentage reduction in voltage during the discharge process, is determined using the following formula:

$$E_r = 1 - E_t = \left(1 - \frac{V_t}{V_0}\right) * 100\% \qquad (8)$$

(2) Percent Residual Voltage (in %), Et

The residual voltage, which represents the percentage of voltage that remains in the battery after discharge, is calculated as follows:

$$E_t = \frac{V_t}{V_0} * 100\% \qquad (9)$$

(3) Discharge Rate (in V/min), Ed

The discharge rate measures the speed at which the battery loses voltage over time. This also signifies the energy released during the discharge process, with a greater voltage drop indicating a more complete discharge. It is determined by dividing the change in voltage by the duration of the discharge process:

$$E_r = \frac{V_0 - V_t}{\Delta t} \qquad (10)$$

Where:

V0 is the initial voltage of battery before discharge, V
Vt is the final voltage of the battery after discharge, V
T is the time of discharge for each run, min

A summary of the DoE with results of the experimental runs is presented in Table 6.

3.4.1 Analysis of each Response Variable with respect to the input variables

Response Variable 1: Voltage Drop

A higher voltage drop indicates a more substantial reduction in the battery's charge, minimizing residual energy and preparing the battery for safe recycling. The impact of the input variables—NaCl concentration (A), discharging time (B), and S/L ratio (C)—on the voltage drop emphasizes significant trends and optimal conditions for the discharging process. Higher NaCl concentrations generally increase the voltage drop, as observed in runs like run 9 (A = 22.73%, Voltage Drop = 58.4%) and run 5 (A = 16%, B = 100.23 mins, Voltage Drop = 59.2%). This enhance-

-ment can be attributed to the improved ionic conductivity provided by the electrolyte, facilitating more efficient electron transfer [81]-[82] during the discharging process [83]. Conversely, lower NaCl concentrations, such as in run 7 (A = 9.27%, Voltage Drop = 56.65%), reduce ionic strength and hinder electrochemical reactions, resulting in slightly lower voltage drops. Hence, higher NaCl concentrations (A > 16%) are preferred for maximizing the discharging process efficiency.

Discharging time (B) significantly influences the percentage voltage drop. Longer times, as seen in run 5 (B = 100.23 mins, Voltage Drop = 59.2%) and run 17 (B = 75 mins, Voltage Drop = 58.68%), allow for more energy dissipation, leading to higher voltage drops [84]. In contrast, shorter discharging times, such as in run 1 (B = 49.77 mins, Voltage Drop = 53.42%), do not provide adequate time for complete energy dissipation, resulting in lower efficiency. Therefore, longer discharging durations (B > 75 mins) are optimal for ensuring thorough and effective energy reduction.

The S/L ratio (C), representing the zinc powder-to-electrolyte ratio, has a significant effect on the voltage drop. Moderate S/L ratios, around 1.4% to 2%, consistently yield higher voltage drops, as seen in run 8 (C = 1.4%, Voltage Drop = 59.32%) and run 10 (C = 2%, Voltage Drop = 53.06%). These values reflect a balance between sufficient catalytic activity and optimal ionic mobility. However, extremely low (C = 0.39%, run 14, Voltage Drop = 56.77%) or high (C = 2.415%, run 6, Voltage Drop = 54.93%) ratios result in suboptimal voltage drops, as they either limit catalytic efficiency or increase viscosity and resistance. Thus, moderate S/L ratios (C = 1.4% - 2.0%) are preferred for achieving efficient catalysis and ionic mobility.

Maximizing the voltage drop is crucial for ensuring the safety and efficiency of the discharging process. A substantial voltage drop ensures that the battery is discharged to a safe state of charge (SOC), minimizing the risk of residual energy causing thermal or chemical hazards. Additionally, lower residual energy levels enhance the efficiency of recycling processes, as less energy dissipation is required during subsequent handling.

Response Variable 2: Residual Voltage, %

The percent residual voltage, which signifies the remaining energy in lithium-ion batteries (LIBs) post-discharge, was systematically evaluated under varying conditions of NaCl concentration (A), discharging time (B), and solid-to-liquid (S/L) ratio (C). These parameters were assessed for their influence on minimizing residual voltage, a critical metric for ensuring safety and enhancing the efficiency of recycling processes. The concentration of NaCl was observed to significantly influence the residual voltage of discharged LIBs. Runs involving higher NaCl concentrations consistently exhibited reduced residual voltage, with values as low as 40.8% recorded at 16% NaCl (run 5). This effect is attributed to the enhanced ionic strength provided by elevated NaCl levels, which facilitates improved conductivity of the electrolyte and accelerates electron transfer[79]. Conversely, lower concentrations, such as 9.27% (run 7), resulted in elevated residual voltages of 43.35%, indicating suboptimal ionic mobility. These findings underscore the importance of maintaining NaCl concentrations above 16% to achieve effective energy dissipation during discharge.

Discharging time demonstrated a proportional relationship with the reduction of residual voltage. Extended discharging periods, exemplified by 100.23 minutes (Run 5), yielded the lowest residual voltage of 40.8%. Shorter discharging durations, as observed in run 1 (49.77 minutes), were associated with significantly higher residual voltage (46.58%), indicative of incomplete energy dissipation. The results suggest that discharging times exceeding 75 minutes is essential to ensure the thorough depletion of stored energy, thereby enhancing the safety and readiness of LIBs for subsequent recycling processes.

The S/L ratio, defined by the proportion of zinc powder to electrolyte, was found to critically impact the discharging efficiency. Moderate ratios, ranging between 1.4% and 2%, achieved the most effective reduction in residual voltage, with values as low as 40.68% (run 8, 1.4%). This balance ensures sufficient catalytic activity while mitigating the adverse effects of excessive viscosity or particle aggregation. Both lower (0.39%, run 14) and higher (2.415%, run 6) ratios led to higher residual voltages, at 43.23% and 45.07%, respectively, due to either insufficient cataly-

-tic presence or hindered ionic mobility. Maintaining the S/L ratio within the 1.4% to 2% range is therefore recommended for optimal performance.

Minimizing residual voltage is crucial to reduce the thermal and chemical risks associated with leftover energy during battery handling and recycling. Batteries discharged under optimal conditions show reduced energy storage, which diminishes the potential for hazardous reactions and ensures safer transportation and processing. Additionally, lower residual voltages improve recycling efficiency, as they require minimal extra energy for battery recovery preparation. The study identifies that NaCl concentrations over 16%, discharging durations exceeding 75 minutes, and solid-to-liquid ratios between 1.4% and 2% are optimal for minimizing residual voltage. These conditions facilitate efficient energy dissipation, promote operational safety, and streamline LIB recycling. The findings highlight the significance of carefully balancing these parameters to optimize the discharging process and align with sustainable recycling objectives.

Response Variable 3: Discharge Rate, V/min

The discharge rate, quantified as the rate of voltage reduction (V/min), is a crucial parameter for assessing the discharging efficiency of lithium-ion batteries (LIBs). A higher discharge rate indicates more rapid energy dissipation, which is critical for ensuring battery safety and readiness for recycling. NaCl concentration impacts the discharge rate by enhancing the ionic conductivity of the electrolyte. Higher concentrations, as seen in run 10 (A = 20%, Discharge Rate = 0.031 V/min) and run 19 (A = 20%, Discharge Rate = 0.031 V/min), improve ionic mobility and reaction kinetics, leading to increased discharge rates. On the contrary, lower concentrations, such as in run 7 (A = 9.27%, Discharge Rate = 0.027 V/min), result in reduced ionic conductivity and slower electrochemical reactions. Therefore, higher NaCl concentrations (A ≥ 16%) are preferred for promoting efficient energy dissipation.

The duration of the discharge process also plays a vital role in determining the discharge rate. Shorter discharging times, such as in run 10 (B = 60 mins, Discharge Rate = 0.031 V/min), are associated with higher discharge rates due to rapid energy release within a condensed timeframe. In contrast, longer discharge times, as seen in run 5 (B = 100.23 mins, Discharge Rate = 0.020 V/min), facilitate a more gradual discharge, resulting in lower rates. Optimal discharging times (B ≈ 60 mins) balance the need for rapid discharge with sufficient time for effective energy dissipation.

The S/L ratio, which represents the proportion of solid to liquid in the electrolyte, affects catalytic activity and ionic mobility. Moderate S/L ratios, such as those in run 3 (C = 2%, Discharge Rate = 0.032 V/min) and run 8 (C = 1.4%, Discharge Rate = 0.028 V/min), yield higher discharge rates by ensuring efficient catalytic activity and maintaining ion mobility. Extreme S/L ratios, like C = 0.39% in run 14 (Discharge Rate = 0.027 V/min) or C = 2.415% in run 6 (Discharge Rate = 0.026 V/min), lead to lower discharge rates due to insufficient catalytic activity or increased resistance from particle aggregation. Thus, moderate S/L ratios (C = 1.4%-2%) are ideal for balancing catalytic efficiency and ionic mobility.

To ensure the efficient and safe discharging of lithium-ion batteries (LIBs), it is crucial to maximize the discharge rate. A high discharge rate allows for rapid energy dissipation, reducing the time required to reach a safe state of charge (SOC) and minimizing the risks associated with residual energy. Achieving this involves optimizing certain conditions, specifically higher NaCl concentrations (≥ 16%), moderate discharging times (around 60 minutes), and solid-to-liquid ratios between 1.4% and 2%. These optimal conditions promote rapid energy dissipation while maintaining safety and efficiency, ensuring that LIBs are effectively discharged and prepared for recycling. By carefully balancing these variables, the discharging process can be made more effective, enhancing overall performance and providing consistent, reliable results for battery preparation.

3.4.2 Statistical Model Analysis of Response Variables

One important part of this study is to be able to quantify the relationships between the variables of the study. Statistical model analysis is essential for comprehending the relationships between input and response variables in experimental studies, especially when optimizing the discharging process of lithium-ion batteries (LIBs). This analysis elucidates how variables like NaCl concentration, discharging time, and S/L ratio affect outcomes such as voltage drop, residual voltage, and discharge rate, thereby guiding data-driven decision-making and optimizing performance. Models like response surface methodology (RSM) quantify the impact of each input variable, revealing key understandings such as the enhancement of ionic conductivity by NaCl concentration and the quadratic effects of discharging time. Crucially, statistical models capture interaction effects between variables, such as the synergistic or antagonistic impacts of NaCl concentration and S/L ratio on discharge rate. Validation metrics like R^2, adjusted R^2, and predicted R^2 ensure the model's reliability in explaining data variability and predicting outcomes, facilitating efficient extrapolation to new variable combinations and saving resources.

Response Variable 1: Percent Voltage Drop

The Fit Summary highlights the model fit for the response variable and is summarized in Table 7. Among the evaluated models (Linear, 2FI, Quadratic, and Cubic), the linear model is suggested based on its p-value (0.2596), indicating a better fit without significant overfitting or aliased parameters. When terms are aliased, it means that there is no unique mathematical way to separate their effects because they overlap entirely with other terms or combinations of terms in the model. The insignificant lack-of-fit (p-value = 0.2911) further supports the Linear model's appropriateness, ensuring the reliability of its predictions. Although the adjusted R2 (0.0744) and predicted R2 (-0.2330) are relatively low, these values reflect the complexity of the interactions between variables and highlight areas for potential refinement in future studies.

In Table 8, the Sequential Model Sum of Squares provides insights into how additional terms influence the model's predictive capacity. The Linear model remains robust, as adding interaction (2FI) or higher-order terms (Quadratic and Cubic) does not yield significant improvements in the F-value or p-value. This suggests that the Voltage Drop is largely governed by independent effects of the input variables rather than complex interactions or non-linear relationships.

Table 7. Fit Summary of the Response 1: Voltage Drop

Source	Sequential p-value	Lack of Fit p-value	Adjusted R^2	Predicted R^2	
Linear	**0.2596**	**0.2911**	**0.0744**	**-0.2330**	**Suggested**
2FI	0.9537	0.2006	-0.1266	-2.1866	
Quadratic	0.2520	0.2231	0.0251	-1.9268	
Cubic	0.8932	0.0417	-0.4547	-60.3293	**Aliased**

Table 8. Sequential Model of Sum for Response 1: Voltage Drop

Source	Sum of Squares	df	Mean Square	F-value	p-value	
Mean vs Total	58545.84	1	58545.84			
Linear vs Mean	**21.35**	**3**	**7.12**	**1.48**	**0.2596**	**Suggested**
2FI vs Linear	1.90	3	0.6321	0.1081	0.9537	
Quadratic vs 2FI	24.62	3	8.21	1.62	0.2520	
Cubic vs Quadratic	7.79	4	1.95	0.2579	0.8932	Aliased
Residual	37.74	5	7.55			
Total	58639.24	19	3086.28			

Table 9. Lack of Fit Test for Response 1: Voltage Drop

Std. Dev.	**2.19**	R^2	**0.2286**
Mean	55.51	**Adjusted R^2**	0.0744
C.V. %	3.95	**Predicted R^2**	-0.2330
		Adeq Precision	3.9852

Fit Statistics in Table 9 further validated the choice of the Linear model. With a standard deviation of 2.19 and an R2 value of 0.2286, the model provides a reasonable explanation for the variance observed in the data. Although the predicted R2 is negative (-0.2330), this could be attributed to noise in the dataset or limited sample size. Further, this indicates that there is limitation with respect to the predictive ability of the model, specifically when applied to typically new and unseen data such as tested range (±α) of the factors (A, B, and C) considered in the study [85]. Despite this, it is also important to note that the Adequate Precision value (3.9852) is just below the threshold of 4, indicating sufficient signal-to-noise ratio for the model's applicability. This fundamentally indicates that the model has enough signal to capture meaningful relationships between the input variables (NaCl concentration, discharging time, Zn powder in NaCl solution) and the response variables (voltage drop, residual voltage, discharge rate)[86].

From the ANOVA results in Table 10, it is evident that discharging time (Factor B) has the most significant effect on Voltage Drop, with a relatively low p-value (0.0629). This aligns with observed trends in the data where extended discharging times (e.g., run 5 with 100.23 mins) correspond to higher Voltage Drops (59.20%). Meanwhile, NaCl concentration (Factor A) and S/L ratio (Factor C) exhibit less direct impact, with p-values of 0.3503 and 0.8106, respectively.

However, their combined influence contributes to the overall optimization. The experimental results validate the statistical analysis, providing details into the influence of input variables on voltage drop during discharge. For NaCl concentration (Factor A), runs 7 (low at 9.27%) and 9 (high at 22.733%) exhibited minimal variation in voltage drop (56.65% and 58.40%, respectively). This consistency indicates that the electrolyte's conductivity is sufficiently enhanced across the tested range, minimizing its influence as a limiting factor.

Discharging time (Factor B) significantly impacted the voltage drop, with run 5 (100.23 minutes) achieving the highest voltage drop of 59.20%. This underscores the importance of sufficient time to ensure complete energy discharge, enhancing safety and effectiveness in battery recycling. For the S/L ratio (Factor C), runs 3 (high at 2.0%) and 14 (low at 0.39%) demonstrated moderate differences, highlighting the catalytic effects of zinc powder. This suggests that the S/L ratio can be fine-tuned to optimize catalytic activity without significant performance variations.

These findings emphasize the critical roles of time and catalyst optimization in achieving maximum voltage drop, ensuring safe and efficient discharging. The results support a systematic approach to optimizing the discharging process for lithium-ion batteries, paving the way for effective recycling. This suggests that the model assumptions hold true, and the variations in voltage drop across the experimental runs are adequately captured. The color-coded points, reflecting different voltage drop values, align with the expected range of variability. On the other hand, the predicted vs. actual plot (Fig. 12) reveals a reasonable agreement between the observed and model-predicted voltage drop values. While there is some scattering around the line of equality, the clustering of points near the diagonal implies the model's capability to capture trends effectively. This alignment reinforces the utility of the model for identifying optimum discharging parameters.

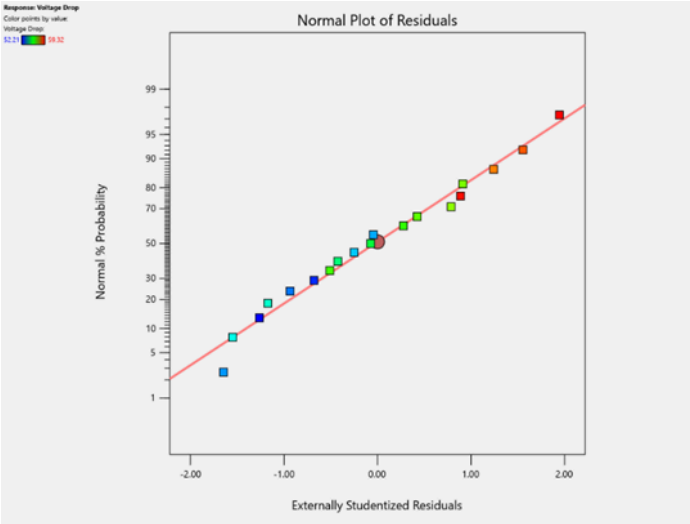

Fig. 11. The normal plots of residuals for Response 1: Voltage Drop

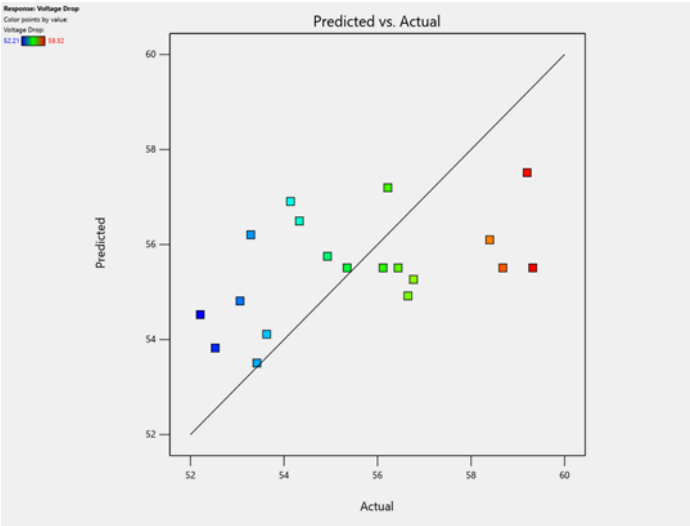

Fig. 12. Predicted vs. Actual Plot for Response 1: Voltage Drop

Furthermore, the residuals vs. NaCl concentration plot (Fig. 13) shows evenly distributed points across the range of NaCl concentrations, with no apparent trend. This indicates that NaCl concentration does not significantly bias the model's predictions, consistent with the minimal impact of Factor A observed in the experimental results.

The results validate the DoE approach by confirming that the model sufficiently explains variations in voltage drop across the experimental conditions. Longer discharging times (Factor B) consistently resulted in higher voltage drops, highlighting time's critical role in achieving optimal discharging. The S/L ratio (Factor C) also influenced the voltage drop, underscoring its catalytic role in optimizing the discharging process. Overall, the diagnostic plots affirm the model's suitability for exploring the discharging process and provide a foundation for optimizing lithium-ion battery recycling protocols. The insights gained are pivotal for fine-tuning operational parameters to achieve efficient and safe discharge.

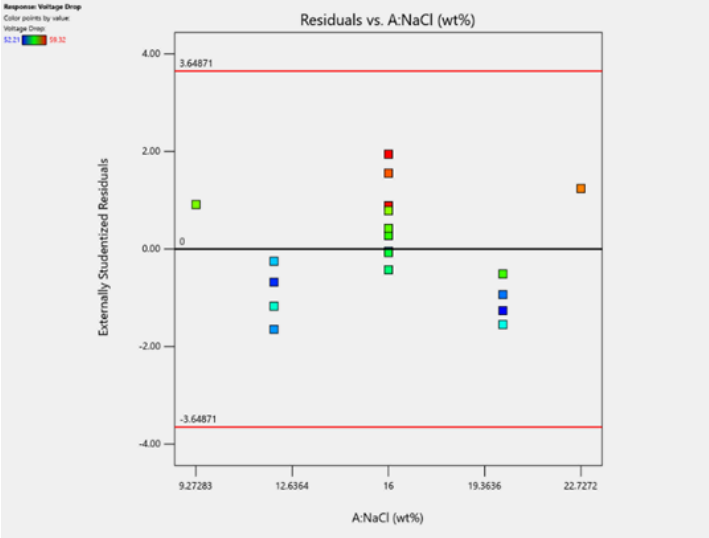

Fig. 13. Predicted vs. NaCl Concentration Plot for Response 1: Voltage Drop

Response Variable 2: Percent Residual Voltage

Given the binomial and inverse nature of percent voltage drop and percent residual voltage, a statistical relationship and some correspondence in the plots are not unexpected. The observed behaviors suggest that as the percent voltage drop increases, the percent residual voltage similarly decreases, which aligns with fundamental electrochemical principles. This inverse relationship can significantly influence the interpretation of model fits, ANOVA results, and subsequent optimization strategies in battery discharge studies.

In the fit summary for response variable 2 similar values and trends are observed as seen in Table 11. A linear model is identified as the best fit for analyzing residual voltage, according to the fit summary. An adjusted R2 value of 0.0744 indicates a weak explanation of variability in the response by the input factors. However, the model's utility is not negated, as the p-values for lack of fit are non-significant (0.2911), indicating that the model fits the data within statistical thresholds. The low R2 value suggests that factors beyond the scope of the experiment might influence residual voltage, calling for additional exploration in future studies. Consequently, Table 12 showing the Sequential Model of Sum Squares also indicated that the linear model exhibits a p-value of 0.2596, indicating that none of the factors significantly impact residual voltage. The absence of significant higher-order interactions (as observed in the quadratic and cubic models) suggests a straightforward relationship between variables, reinforcing the selection of the linear model. Further, the ANOVA (Table 13) and Fit Statistics (Table 14) of the response variable 2 indicates that Factor B (discharging time) approaches significance ($p = 0.0629$), suggesting that extended discharge times contribute to lower residual voltage. Factors

A (NaCl concentration) and C (S/L ratio) exhibit p-values far from significance, confirming minimal influence on residual voltage.

This trend aligns with experimental runs where time was critical for achieving optimal battery discharge levels; and despite the low adjusted R2 and predicted R2 values, the adequate precision of 3.9852 meets the reliability threshold for this type of study. This ensures that the model predictions, while limited, remain credible within the context of the design space.

Table 11. Fit Summary for Response 2: Residual Voltage

Source	Sequential p-value	Lack of Fit p-value	Adjusted R^2	Predicted R^2	
Linear	**0.2596**	**0.2911**	**0.0744**	**-0.2330**	**Suggested**
2FI	0.9537	0.2006	-0.1266	-2.1866	
Quadratic	0.2520	0.2231	0.0251	-1.9268	
Cubic	0.8932	0.0417	-0.4547	-60.3293	**Aliased**

Table 12. Sequential Model Sum of Squares for Response 2: Residual Voltage

Source	Sum of Squares	df	Mean Square	F-value	p-value	
Mean vs Total	37607.84	1	37607.84			
Linear vs Mean	**21.35**	**3**	**7.12**	**1.48**	**0.2596**	**Suggested**
2FI vs Linear	1.90	3	0.6321	0.1081	0.9537	
Quadratic vs 2FI	24.62	3	8.21	1.62	0.2520	
Cubic vs Quadratic	7.79	4	1.95	0.2579	0.8932	Aliased
Residual	37.74	5	7.55			
Total	37701.24	19	1984.28			

Variations in NaCl concentration, as observed in runs 7 (low concentration) and 9 (high concentration), did not significantly alter residual voltage percentages, indicating that the electrolyte's conductivity remains effective across the tested range. run 5, with a discharging time of 100.23 minutes, exhibited the lowest residual voltage at 40.8%, underscoring the importance of longer discharging times for thorough depletion. Meanwhile, runs with high (run 3) and low (run 14) S/L ratios reflect only minor fluctuations in residual voltage, suggesting that the S/L ratio is less critical compared to discharge time.

These insights highlight the robustness of the Design of Experiments (DoE) in defining the influence of key factors. Although the statistical significance is modest, the model reliably identifies discharge time as the most impactful variable, guiding further optimization efforts. Consequently, these results will inform the refinement of discharging protocols to ensure lithium-ion batteries are safely and efficiently prepared for recycling.

Table 13. ANOVA for linear model Response 2: Residual Voltage

Source	Sum of Squares	df	Mean Square	F-value	p-value	
Model	21.35	3	7.12	1.48	0.2596	not significant
A-NaCl	1.68	1	1.68	0.3503	0.5628	
B-Time	19.38	1	19.38	4.04	0.0629	
C-Zn in NaCl Solution	0.2858	1	0.2858	0.0595	0.8106	
Residual	72.04	15	4.80			
Lack of Fit	60.19	11	5.47	1.85	0.2911	not significant
Pure Error	11.85	4	2.96			
Cor Total	93.40	18				

Table 14. Fit Statistics for Response 2: Residual Voltage

Std. Dev.	**2.19**	**R^2**	**0.2286**
Mean	44.49	**Adjusted R^2**	0.0744
C.V. %	4.93	**Predicted R^2**	-0.2330
		Adeq Precision	3.9852

Diagnostic Plots for Percent Residual Voltage

Fig. 14 shows that in the normal probability plot for percent residual voltage, the residuals align closely with the expected normal distribution. Minor deviations exist, yet the plot indicates that residuals are mostly normally distributed, thereby validating the linear model's assumptions. The color gradient from blue to red reflects the range of residual voltage, emphasizing a well-spread but systematic variability. Further, the model predictions align closely with experimental results as seen in the predicted versus actual values plot (Fig. 15). Although not perfect, the model captures the general trend effectively, as evidenced by the slight scattering around the ideal line. The color-coding indicates that higher residual voltages (orange and red) are predicted slightly less accurately, suggesting potential areas for model refinement or further optimization of significant factors.

The plot of externally studentized residuals against NaCl concentration in Fig. 16 shows consistency across NaCl levels, with minimal outliers. Residuals generally fall within acceptable thresholds, confirming the model's robustness in predicting percent residual voltage across varying NaCl concentrations. Despite a relatively low Adjusted R^2 (0.0744), the model offers meaningful insights, especially when viewed alongside the diagnostic plots. The design of experiments (DoE) results suggests that discharging time (Factor B) significantly influences percent residual voltage. For instance, longer durations, such as run 5 (100.23 minutes), yield lower residual voltages, underscoring the importance of sufficient discharge time.

Overall, the statistical model aligns predictions with experimental results and demonstrates utility in optimizing lithium-ion battery discharging for recycling. This model highlights the potential for further accuracy refinement and emphasizes the importance of time in improving discharging outcomes.

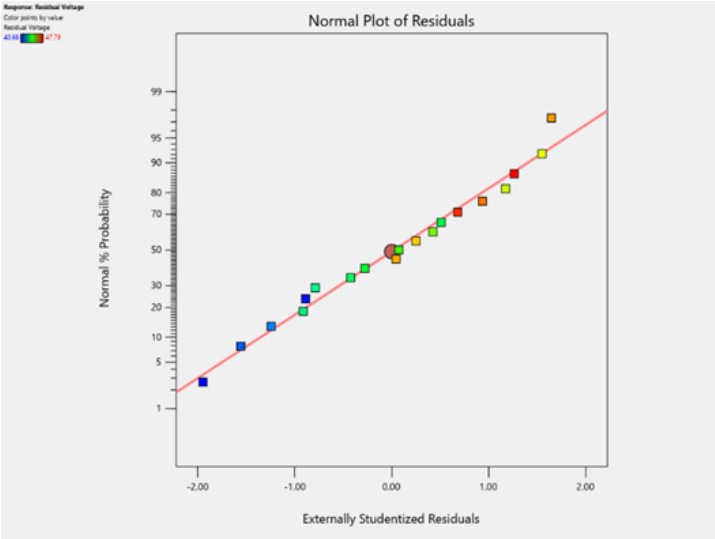

Fig. 14. Normal plot of residuals for Response 2: Residual Voltage

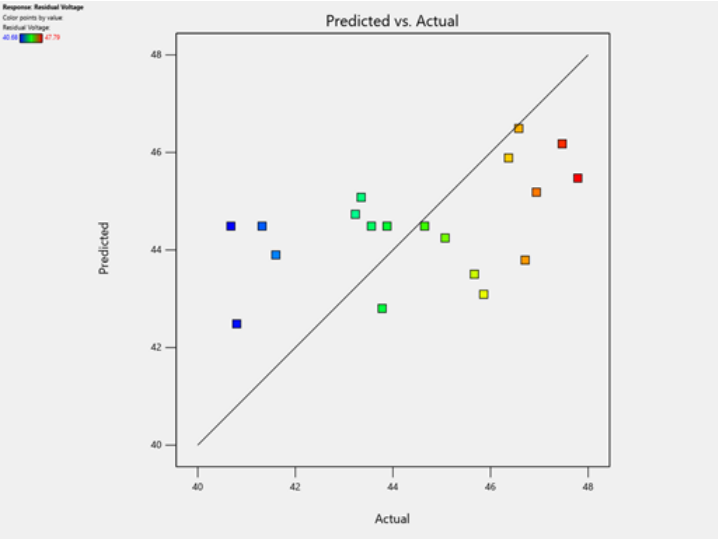

Fig. 15. Predicted vs. Actual values for Response 2: Residual Voltage

Response Variable 3: Discharge Rate

Table 15 presents that the linear model is recommended due to its significant sequential p-value (< 0.0001) and acceptable lack-of-fit p-value (0.2190). The adjusted R^2 value of 0.9547 and predicted R^2 value of 0.9343 confirm its strong predictive power, demonstrating reliability in capturing the relationships between input variables and the discharge rate.

This is in support of the ANOVA for the Linear Model (Table 16) that indicates statistical significance (p-value < 0.0001), showing that the factors effectively explain variability in discharge rate. Factor B (Discharging Time) is the most impactful variable, with a highly significant p-value (< 0.0001), suggesting that longer discharging times are critical for achieving higher discharge rates. Factors A (NaCl concentration) and C (Zn in NaCl solution) show less influence, as their p-values exceed the 0.05 threshold. The Fit Statistics (Table 17) further displays the robustness of the model, with a low standard deviation (0.0010) and an Adequate Precision value of 38.7137, confirming a strong signal-to-noise ratio suitable for optimization.

Table 6 (summary of DoE) supports these inferences, showing that runs with longer discharging times (e.g., run 5 with 100.23 minutes) exhibit relatively stable discharge rates. This suggests that optimizing discharging time enhances process efficiency. Despite some variabi-

-lity in other factors, the model effectively predicts discharge rate trends and provides a reliable framework for refining the discharging process. This ultimately shows that the model highlights discharging time as the key factor influencing discharge rate. Its high predictive accuracy and statistically significant findings provide a solid foundation for optimizing lithium-ion battery discharging processes, ensuring safe and efficient recycling operations.

Diagnostic Plots for Discharge Rate

The normal probability plot for residuals (Fig. 18) illustrates a close alignment with the theoretical normal distribution, as most data points are situated near the diagonal line. While minor deviations occur at the extremes, these do not significantly impact the model's validity, thereby confirming that the assumption of normally distributed residuals is satisfied. This ensures that the model's predictions remain unbiased and reliable across the tested range, despite the slight non-normality or potential outliers observed at the tails. In Fig. 19, the predicted versus actual plot demonstrates strong agreement between the predicted discharge rate and the actual experimental values. Data points are clustered around the diagonal line, indicating minimal deviation between the predicted and actual discharge rates. This alignment underscores the model's reliability and predictive accuracy. Though, there is a slight scatter observed in a few data points—indicating some minor residuals remain unexplained—this scatter suggests that while the model successfully captures most of the variability, it does not account for every possible variation.

Table 15. Fit Summary for Response 3: Discharge Rate

Source	Sequential p-value	Lack of Fit p-value	Adjusted R^2	Predicted R^2	
Linear	**< 0.0001**	**0.2190**	**0.9547**	**0.9343**	**Suggested**
2FI	0.9555	0.1469	0.9448	0.8951	
Quadratic	0.0869	0.2535	0.9633	0.8917	
Cubic	0.9438	0.0433	0.9419	-1.4313	**Aliased**

Table 16. ANOVA for Linear Model for Response 3: Discharge Rate

Source	Sum of Squares	df	Mean Square	F-value	p-value	
Model	0.0004	3	0.0001	127.36	< 0.0001	significant
A-NaCl	6.590E-07	1	6.590E-07	0.6748	0.4242	
B-Time	0.0004	1	0.0004	380.87	< 0.0001	
C-Zn in NaCl Solution	5.266E-07	1	5.266E-07	0.5393	0.4741	
Residual	0.0000	15	9.766E-07			
Lack of Fit	0.0000	11	1.150E-06	2.30	0.2190	not significant
Pure Error	2.000E-06	4	5.000E-07			
Cor Total	0.0004	18				

Table 17. Fit Statistics for Response 3: Discharge Rate

Std. Dev.	**0.0010**	R^2	**0.9622**
Mean	0.0269	**Adjusted R^2**	0.9547
C.V. %	3.67	**Predicted R^2**	0.9343
		Adeq Precision	38.7137

These unexplained residuals might result from unaccounted experimental factors, inherent noise in the data, or minor deviations in the experimental conditions. Despite these minor discrepancies, the model still provides a consistent prediction framework for discharge rates, highlighting areas for potential refinement and optimization in future experiments.

The plot of externally studentized residuals against NaCl concentration (Fig. 19) reveals no discernible pattern or trend, as the residuals are randomly distributed around zero. This randomness indicates that the model does not systematically over- or under-predict the discharge rate across different levels of NaCl concentration, supporting the assumption of homoscedasticity. Homoscedasticity implies that the variance of residuals remains consistent across the range of Factor A, in this case, NaCl concentration. The consistent variance ensures that the model's predictive accuracy is not influenced by the concentration of NaCl, providing reliable predictions regardless of this factor's level.

Additionally, the absence of clustering or patterns in the residuals suggests that NaCl concentration does not have a significant impact on the discharge rate. This observation aligns with the ANOVA results, which indicated that Factors B (Discharging Time) and C (Zn in NaCl solution) have more substantial effects on the discharge rate than NaCl concentration. Consequently, the model's consistency and predictive reliability are further confirmed, as it accurately captures the relationship between the discharge rate and the varying levels of NaCl concentration, without being biased by this factor.

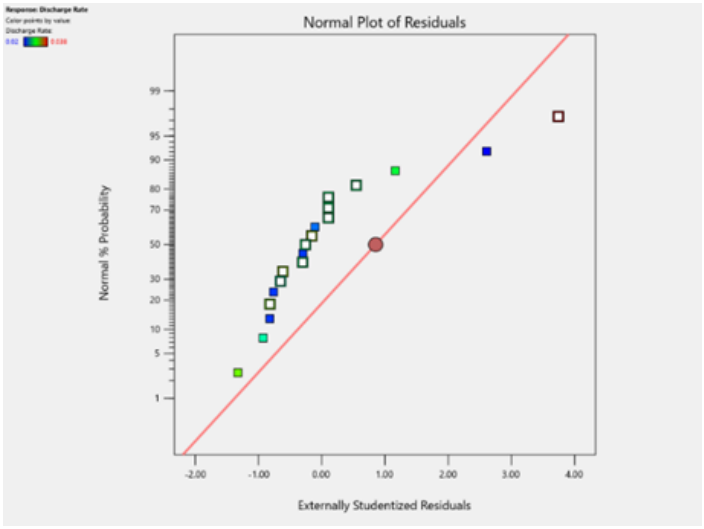

Fig. 17. Normal Plot of residuals for Response 3: Discharge Rate

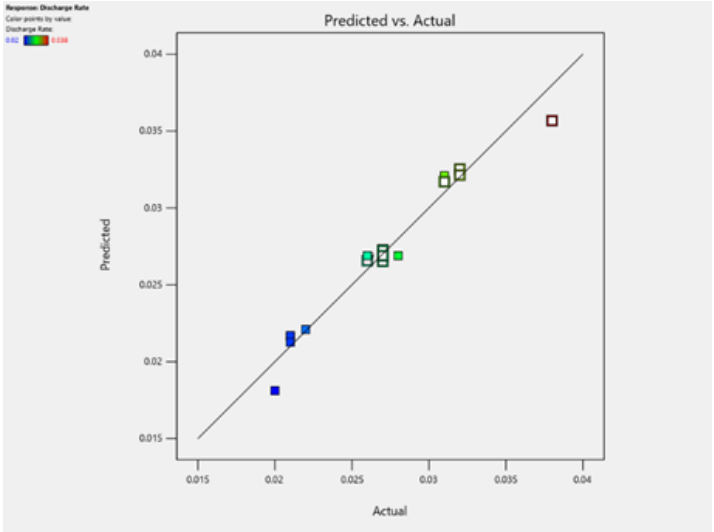

Fig. 18. Predicted vs Actual Plot for Response 3: Discharge Rate

The diagnostic plots were collectively analyzed to confirm the assumptions of normality, linearity, and homoscedasticity for the model. The findings indicated that the linear model provides an accurate and reliable representation of the discharge rate, with minimal systematic bias. The evaluation of these diagnostic plots also reinforced the statistical insignificance of NaCl concentration as a factor, thereby shifting the focus toward the optimization of other significant parameters such as discharge time (Factor B).

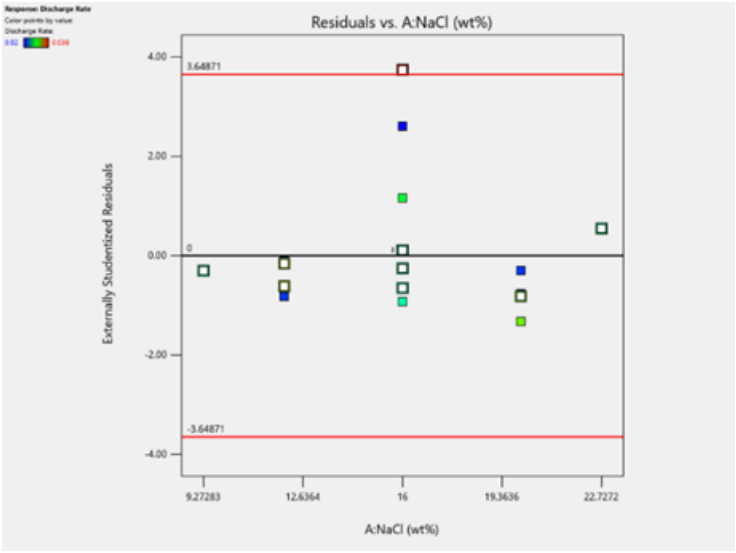

Fig. 19. Residuals vs. NaCl Concentration for Response 3: Discharge Rate

The comprehensive assessment of the diagnostic plots instilled confidence in the model's ability to generalize effectively, ensuring its utility in guiding process optimization. By confirming that the model's assumptions are valid, it was ascertained that the predictions are unbiased and reliable across the tested range. The minor deviations and potential outliers observed in the plots did not undermine the model's validity, further supporting its robustness.

The thorough examination of the diagnostic plots validated the linear model, highlighting the importance of optimizing significant parameters like discharge time while confirming the negligible impact of NaCl concentration. This comprehensive evaluation affirms the model's efficacy in predicting discharge rates and guiding the optimization of lithium-ion battery discharging processes for recycling operations.

Summary

The analysis of the statistical model reveals that Factor B (Discharge Time) is the predominant factor significantly influencing the system's performance, particularly concerning key response variables such as Voltage Drop and Discharge Rate. This finding suggests that the duration of the discharge process is critical in achieving optimal outcomes and should, therefore, be prioritized during process optimization.

The analysis indicates that variations in NaCl concentration (Factor A) have a relatively minimal impact on the response variables. This observation suggests that, within the tested range, the electrolyte's conductivity is sufficiently enhanced, and further changes in concentration are unlikely to yield substantial improvements. The stability in the performance of NaCl concentration implies that this factor is already operating within a functional range that supports the process efficiently.

To leverage this insight, it is recommended that the NaCl concentration be maintained at a stable, optimal baseline level to ensure consistent electrolyte performance. Additional studies might explore concentrations beyond the tested range to confirm this trend or uncover new behaviors at extreme levels. However, significant efforts to adjust this factor may not be warran-

-ted at this stage.

Factor C, the solid-to-liquid ratio, exhibits a moderate influence on Voltage Drop and Residual Voltage but has limited impact on Discharge Rate. This finding suggests that, while this factor does not drive the system's overall performance, it can serve as a secondary tuning parameter. By carefully adjusting the solid-to-liquid ratio, subtle catalytic effects and material interactions may be optimized, leading to incremental improvements in specific response variables.

Table 18. Summary of coded equations for all response variables

Response Variable	Coded Equation
[1] Percent Voltage Drop	$\hat{y}_1 = +55.51 + 0.3510\,\mathbf{A} + 1.19\,\mathbf{B} + 0.1447\,\mathbf{C}$
[2] Percent Residual Voltage	$\hat{y}_2 = +44.49 - 0.3510\,\mathbf{A} - 1.19\,\mathbf{B} - 0.1447\,\mathbf{C}$
[3] Discharge Rate	$\hat{y}_3 = +0.0269 - 0.0002\,\mathbf{A} - 0.0052\,\mathbf{B} - 0.0002\,\mathbf{C}$

Table 19. Summary of actual equations for all response variables

Response Variable	Actual Equations
[1] Percent Voltage Drop	$\hat{y}_1 = +47.81160 + 0.087742\,\mathbf{A} + 0.079427\,\mathbf{B} + 0.241088\,\mathbf{C}$
[2] Percent Residual Voltage	$\hat{y}_2 = +52.18840 - 0.087742\,\mathbf{A} - 0.079427\,\mathbf{B} - 0.241088\,\mathbf{C}$
[3] Discharge Rate	$\hat{y}_3 = +0.054326 - 0.000055\,\mathbf{A} - 0.000348\,\mathbf{B} - 0.000327\,\mathbf{C}$

For Factor C, targeted investigations are recommended to identify the most cost-effective and operationally efficient ratio. This approach would allow process optimization to minimize waste or reduce costs while ensuring that other critical parameters, such as Voltage Drop, remain within desirable ranges.

The dominance of Discharge Time (Factor B) highlights its importance within the overall system. Efforts should be focused on pinpointing the exact discharge durations that maximize Voltage Drop and Discharge Rate without compromising the stability of the system or increasing energy costs. Since Factors A and C show less influence, they should be treated as supporting parameters to the optimization of Factor B. Their ranges can be narrowed down based on the current findings to reduce experimental variability and ensure consistent results in future trials.

3.5 Mathematical models for the response variables

One of the objectives of the study is to produce a mathematical model for each response variable with respect to the input variable identified. In design expert, two types of equations are generated namely: (1) Coded Equations and (2) Actual Equations.

Coded equations use normalized variables to allow for unbiased comparisons of factors' importance and simplify sensitivity analysis, highlighting significant impacts during optimization. They enable researchers to identify dominant factors and interactions without the influence of units an scales. On the other hand, actual equations retain the variables' original units, making them essential for practical applications. They allow practitioners to adjust process parameters precisely, ensuring optimal operation based on specific requirements [68], [87]. The combination of coded and actual equations provides a comprehensive appro-

-ach: coded equations aid theoretical analysis, while actual equations ensure practical implementation, bridging experimental design and real-world application effectively [88].

A summary of the coded equations is presented in table 18. Across all response variables, time (B) was identified as the dominant factor across all responses, significantly influencing the outcomes. For Percent Voltage Drop, Time (B) exhibited the highest positive coefficient, indicating that longer discharge times effectively increase the voltage drop. Similarly, for Percent Residual Voltage, Time (B) showed the strongest negative influence, suggesting that extended durations reduce the residual voltage more effectively than the other factors. In contrast, NaCl concentration (A) and Zn in NaCl solution (C) demonstrated smaller coefficients, indicating their relatively less impact on the responses. Although these factors contributed to changes in the outcomes, their effects were overshadowed by the influence of Time (B). For Discharge Rate, the coded equation revealed minimal variations, with all factors, including Time (B), displaying small coefficients. This finding suggests that the discharge rate is less sensitive to the tested factor levels compared to the other responses.

Subsequently, Table 19 shows the summary of the final equation in terms of actual factors. For Percent Voltage Drop, a positive correlation with all three factors is observed. Zn in NaCl solution exhibits the strongest influence, as indicated by the coefficient (+0.241088), followed by time (+0.079427) and NaCl concentration (+0.087742). This implies that increasing these factors enhances the voltage drop, with Zn in NaCl solution having the most significant impact. Percent Residual Voltage shows an inverse relationship for all factors, reflected by negative coefficients. The strongest effect is again from Zn in NaCl solution (-0.241088), significantly reducing residual voltage. Time (-0.079427) and NaCl concentration (-0.087742) also contribute to the reduction, though to a lesser extent. For Discharge Rate, the factors have negligible effects, as evidenced by the small coefficients for NaCl concentration (-0.000055), time (-0.000348), and Zn in NaCl solution (-0.000327). This indicates that these factors do not substantially impact the discharge rate within the experimental range.

Table 20. Summary of criteria of the case study variables and its goals

Name	Goal	Lower Limit	Upper Limit	Importance
A: NaCl	is in range	12	20	3
B: Time	maximize	60	90	5
C: Zn in NaCl Solution	maximize	0.8	2	4
Voltage Drop	maximize	52.21	59.32	4
Residual Voltage	minimize	40.68	47.79	4
Discharge Rate	is in range	0.02	0.038	3

Table 21. Summary of Top 10 Solutions on the optimized study with the set criteria

	NaCl	Time	Zn in NaCl Solution	Voltage Drop	Residual Voltage	Discharge Rate	Desirability
1	**20.000**	**90.000**	**2.000**	**57.197**	**42.803**	**0.021**	**0.846**
2	19.934	90.000	2.000	57.191	42.809	0.021	0.846
3	19.970	89.964	2.000	57.192	42.808	0.021	0.846
4	19.769	90.000	2.000	57.177	42.823	0.021	0.845
5	20.000	90.000	1.989	57.194	42.806	0.021	0.844
6	20.000	89.862	2.000	57.186	42.814	0.021	0.844
7	19.707	90.000	2.000	57.171	42.829	0.021	0.844
8	19.635	90.000	2.000	57.165	42.835	0.021	0.844
9	19.568	90.000	2.000	57.159	42.841	0.021	0.843
10	19.475	90.000	2.000	57.151	42.849	0.021	0.843

The critical role of Zn in NaCl solution in influencing both percent voltage drops, and residual voltage is highlighted, necessitating prioritization of adjustments to this factor for optimizing battery performance. Its dual effect—enhancing voltage drop and reducing residual voltage—underscores its importance. Time is identified as the second most influential factor for both voltage drop and residual voltage. Its significance in ensuring effective discharge is emphasized, with longer durations potentially providing more complete discharge. However, this must be balanced against operational constraints. The minimal impact of NaCl concentration and the discharge rate equation suggest that changes to this factor or response within the tested range might have limited effects. Therefore, it can be maintained at practical levels without compromising performance.

The primary difference between coded and actual equations lies in their purpose and scaling. Coded equations standardize factor levels to a range of -1 to +1, highlighting the relative importance of factors within the experimental design. This approach identifies time (Factor B) as the dominant factor due to its significant impact across the design space. Conversely, actual equations retain the original units of the factors, emphasizing real-world applicability. In this context, Zn in NaCl solution (Factor C) appears most influential, as reflected by its scaled coefficients.

This difference arises from the scaling and normalization in coded equations versus the real-world interpretation of actual equations. Coded equations are useful for theoretical insights and understanding the importance of factors, while actual equations are more practical for predicting outcomes and implementing adjustments in real-world scenarios. Both perspectives are complementary. Time (Factor B) is crucial for optimizing discharge processes in experimental analysis, while Zn in NaCl solution (Factor C) should be prioritized in real-world applications due to its substantial influence on Percent Voltage Drop and Residual Voltage. This dual approach ensures a comprehensive strategy for both experimental design and practical implementation.

3.6 Model validation through optimization studies using desirability functions in Design-Expert®

Another feature of the Design-Expert® is that optimization studies—in response to the interpretations of the statistical model analyses—can be done to check whether the assigned conditions for optimizations have high desirability. In these optimization case studies, the researcher will have to set the constraints and establish goals (maximize, minimize, target, in range, equal to) for the variables (factors and responses). A summary of the constraints for the optimized study is summarized in Table 20.

Table 22. Desirability scale as defined by Harrington

Scale of D	Quality Evaluation
1.00	Improvement beyond this point has no preference
1.00 – 0.80	Acceptable and excellent
0.80 – 0.63	Acceptable but good
0.63 – 0.40	Acceptable but poor
0.40 – 0.30	Borderline
0.30 – 0.00	Unacceptable
0.00	Completely unacceptable

3.6 A. Model validation through optimization studies using desirability functions in Design-Expert®

The goals for each of the variables are set in reference to the findings of the statistical model analysis and relationships of the variables. For these factors, it has been determined that NaCl concentration (A) should be maintained within range due to its minimal impact on the responses. Ensuring it stays within practical limits supports efficient operations without compromising performance. Time (B), identified as the dominant factor, should be maximized to enhance the Percent Voltage Drop and reduce Percent Residual Voltage, both of which are critical for battery performance. Similarly, Zn in NaCl solution (C) should also be maximized to leverage its strong positive influence on Voltage Drop and its negative impact on Residual Voltage, making it a key variable for optimization.

Regarding the responses, the goal for Percent Voltage Drop is to maximize it, as a high voltage drop reflects effective discharge, which is crucial for safe recycling and optimal functionality. The goal for Percent Residual Voltage is to minimize it, ensuring the discharge process is nearly complete, thereby reducing inefficiencies and energy remnants. The discharge rate should remain within range, as it shows minimal sensitivity to the factors, and maintaining it within practical bounds avoids operational disruptions.

To implement these goals, the optimization strategy involves integrating them into a desirability function within Design-Expert software. Relative importance is assigned to each goal, prioritizing critical objectives like maximizing Voltage Drop and minimizing Residual Voltage. Numerical optimization is then conducted to identify the combination of factors that achieve the highest overall desirability while adhering to operational constraints and ensuring practical applicability. The top ten solutions (out of 68) with the highest desirability are summarized in Table 21.

In the software, desirability is an objective function that quantifies how well a solution meets the defined optimization criteria, ranging from 0 (undesirable) to 1 (optimal). During numerical optimization, the software searches for a combination of factor levels that maximizes the overall desirability function, ensuring the best possible outcome for multiple responses. When optimizing multiple responses simultaneously, Design-Expert integrates all individual desirability values into a single composite function, enabling a balanced solution that best satisfies the predefined objectives [89].

This approach is consistent with the desirability function introduced by Derringer and Suich early in the 1980's which was then commonly used in optimization for processes or studies involving simultaneous responses to be optimized. In this method, each set of responses obtained by applying an experimental design is transformed into dimensionless values called individual desirability (di), which are then aggregated into a single response called overall desirability (D). Consequently, an experimental condition that best meets the user's needs with respect to the evaluated responses is likely to be identified through this approach[90].

The set goals for each variable have produced an optimal factor level of: 20wt.% NaCl concentration; 90 mins discharge time; and 2wt.% Zinc in NaCl solution slurry for the discharging process and resulting to a predicted response of: 57.197% voltage drop, 42.803% residual voltage, and 0.021 V/min of discharge rate with a desirability of 0.846 or 84.6%. In this context, the desirability function aggregates the individual desirability for each response, based on their respective optimization goals. A desirability of 0.846 indicates that the selected conditions meet the optimization criteria very well and are considered acceptable and excellent[90] as reflected in Table 22, although they may still achieve perfect alignment with all the specified goals. These variations in responses are remarkably reflected in the actual results in run 15 of Table 6 where the exact same conditions (20wt.% NaCl concentration; 90 mins discharge time; and 2wt.% Zinc in NaCl solution slurry) produced the following response of: 56.22% voltage drop, 43.78% residual voltage, and 0.021 V/min. The comparison of the predicted values and the values is summarized in Table 23 and Fig. 20.

Table 23. Summary of the predicted values from the optimized conditions generated by the Design-Experts desirability function vs. actual values from run 05 of the DoE, at 84.6% desirability

	Factors			Response		
	A wt.%	B mins.	C wt.%	R1 %	R2 %	R3 V/min
Solution 1 (Predicted Values)	20	90	2	57.197	42.803	0.021
Run 15 (Actual Values	20	90	2	56.22	43.78	0.021

The actual responses validate the model and its statistical predictions. The small differences between predicted and actual values are within an acceptable range, supporting the reliability of the model for making predictions under similar experimental conditions. The deviation in the actual Voltage Drop (56.22%) and Residual Voltage (43.78%) compared to predictions is minimal (less than 2%). This small deviation is expected in experimental setups due to inherent variability and noise in the data. Such deviations are within acceptable error margins, particularly when considering the high desirability of 0.846, which indicates the optimization process used in Design-Expert is reliable and consistent with the statistical model analyses.

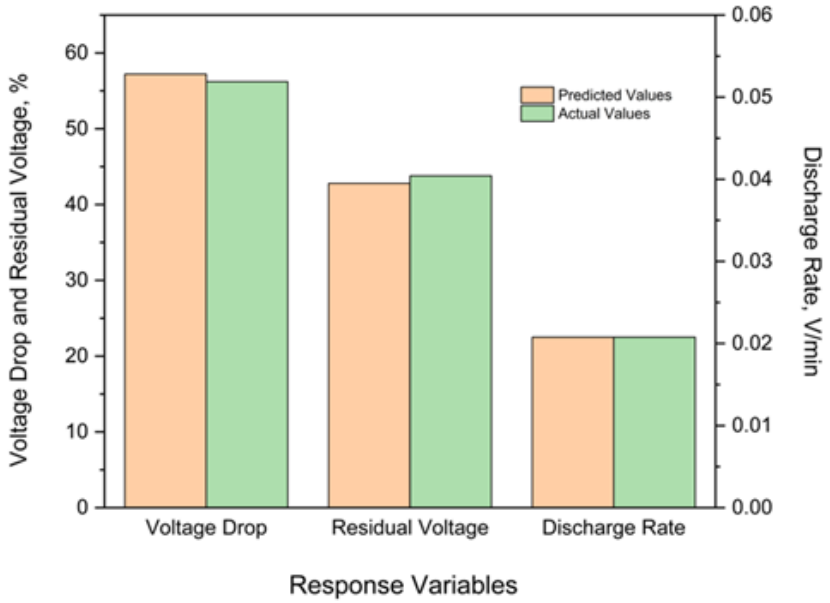

Fig. 20. A bar graph showing the comparison of the predicted and actual values to validate the generated actual equation for the responses: voltage drop, residual voltage, and discharge rate.

4 CONCLUSIONS AND FUTURE WORKS

The optimization of the discharging process for lithium-ion batteries using zinc powder as a catalyst was successfully achieved through Response Surface Methodology (RSM). A robust Design of Experiment (DoE) was developed using Central Composite Design (CCD) of the Design-Expert® software, incorporating NaCl concentration, discharge time, and Zn in NaCl solution as independent variables. on key parameters: Percent Voltage Drop (Er), Residual Voltage Percent (Et), and Discharge Rate (Ed). The DoE effectively captured the voltage profiles of experimental runs, demonstrating the interplay between the factors and their influence on the discharging process.

It was revealed through statistical analysis that discharge time (B) is the dominant factor in driving Percent Voltage Drop and Residual Voltage, as highlighted by coded equations. In real-world applications, Zn in NaCl solution (C) emerged as the most impactful variable, significantly enhancing Voltage Drop and minimizing Residual Voltage, as shown by the actual equations. NaCl concentration (A) had a smaller but consistent influence, supporting its maintenance within practical operational ranges. The lack of significant synergistic or antagonistic effects simplified the optimization process, enabling a focus on independent factor contributions.

Coded and actual model equations for Percent Voltage Drop, Residual Voltage, and Discharge Rate were successfully formulated using Design-Expert® with respect to the results of the 19 experimental runs as DoE. The actual models have provided reliable predictions with minimal deviations from actual experimental results.

These models were validated through the conduct of optimization studies using the software's desirability function where goals were set to for the factors and responses producing solutions with corresponding desirability. Based on the goals set, the optimal conditions for the discharging process were identified and translated to a less than 2% variation in the actual values for the response with a desirability of 0.846. solidifying the reliability of the models in the tested range.

Considering these conclusions, future studies should explore the scalability and industrial applications of the proposed discharging setup. Scaling up the discharging process may face challenges such as increased electrolyte volume, uneven electrode reactions, and operational inefficiencies in continuous processing. These can be addressed by: (1) integration with advanced recycling processes; (2) investigations into alternative catalysts; (3) real-time monitoring systems, can further enhance discharging efficiency; (4) design external discharging set-up flexible to different battery formats (e.g., cylindrical, pouch cells, prismatic, etc.). Additionally, expanding the study to other LIB chemistries and battery types would broaden the applicability of the findings of the optimization studies.

REFERENCES

{1] "Lithium-Ion Battery - Clean Energy Institute." Accessed: Jul. 22, 2024. [Online]. Available: https://www.cei.washington.edu/research/energy-storage/lithium-ion-battery/
[2] D. Steward, A. Mayyas, and M. Mann, "Economics and Challenges of Li-Ion Battery Recycling from End-of-Life Vehicles," Procedia Manuf., vol. 33, pp. 272–279, Jan. 2019, doi: 10.1016/j.promfg.2019.04.033.
[3] H. (Claire) Xiong, E. J. Dufek, and K. L. Gering, "2.20 Batteries," in Comprehensive Energy Systems, Elsevier, 2018, pp. 629–662. doi: 10.1016/B978-0-12-809597-3.00245-5.
[4] L. Li et al., "The Recycling of Spent Lithium-Ion Batteries: a Review of Current Processes and Technologies," Electrochem. Energy Rev., vol. 1, no. 4, pp. 461–482, Dec. 2018, doi: 10.1007/s41918-018-0012-1.
[5] J. T. Warner, Lithium-Ion Battery Chemistries: A Primer. Cambridge, MA: Elsevier, 2019.
[Appl. Surf. Sci. Adv., vol. 9, p. 100233, Jun. 2022, doi: 10.1016/j.apsadv.2022.100233.

[6] UL Research Institutes, "What Are Lithium-Ion Batteries?," UL Research Institutes. Accessed: Apr. 03, 2023. [Online]. Available: https://ul.org/research/electrochemical-safety/getting-started-electrochemical-safety/what-are-lithium-ion
[7] A. Mishra et al., "Electrode materials for lithium-ion batteries," Mater. Sci. Energy Technol., vol. 1, no. 2, pp. 182–187, Dec. 2018, doi: 10.1016/j.mset.2018.08.001.
[8] T. M. Higgins et al., "A Commercial Conducting Polymer as Both Binder and Conductive Additive for Silicon Nanoparticle-Based Lithium-Ion Battery Negative Electrodes," ACS Nano, vol. 10, no. 3, pp. 3702–3713, Mar. 2016, doi: 10.1021/acsnano.6b00218.
[9] P. Sengodu and A. D. Deshmukh, "Conducting polymers and their inorganic composites for advanced Li-ion batteries: a review," RSC Adv., vol. 5, no. 52, pp. 42109–42130, 2015, doi: 10.1039/C4RA17254J.
[10] P. U. Nzereogu, A. D. Omah, F. I. Ezema, E. I. Iwuoha, and A. C. Nwanya, "Anode materials for lithium-ion batteries: A review," Appl. Surf. Sci. Adv., vol. 9, p. 100233, Jun. 2022, doi: 10.1016/j.apsadv.2022.100233.
[11] Z. Yan et al., "Co 3 O 4 /Co nanoparticles enclosed graphitic carbon as anode material for high performance Li-ion batteries," Chem. Eng. J., vol. 321, pp. 495–501, Aug. 2017, doi: 10.1016/j.cej.2017.03.146.
[12] C. Zhang et al., "Challenges and Recent Progress on Silicon-Based Anode Materials for Next-Generation Lithium-Ion Batteries," Small Struct., vol. 2, no. 6, p. 2100009, Jun. 2021, doi: 10.1002/sstr.202100009.
[13] N. Nitta, F. Wu, J. T. Lee, and G. Yushin, "Li-ion battery materials: present and future," Mater. Today, vol. 18, no. 5, pp. 252–264, Jun. 2015, doi: 10.1016/j.mattod.2014.10.040.
[14] X. Li et al., "Study of Lithium Silicide Nanoparticles as Anode Materials for Advanced Lithium Ion Batteries," ACS Appl. Mater. Interfaces, vol. 9, no. 19, pp. 16071–16080, May 2017, doi: 10.1021/acsami.6b16773.
[15] S. H. Oh, O. H. Kwon, Y. C. Kang, J.-K. Kim, and J. S. Cho, "Highly integrated and interconnected CNT hybrid nanofibers decorated with α-iron oxide as freestanding anodes for flexible lithium polymer batteries," J. Mater. Chem. A, vol. 7, no. 20, pp. 12480–12488, 2019, doi: 10.1039/C9TA01374A.
[16] J. Y. Han and S. Jung, "Thermal Stability and the Effect of Water on Hydrogen Fluoride Generation in Lithium-Ion Battery Electrolytes Containing LiPF6," Batteries, vol. 8, no. 7, p. 61, Jun. 2022, doi: 10.3390/batteries8070061.
[17] I. Gunawan, Deswita, B. Sugeng, and Sudaryanto, "Synthesis and characterization of PVA blended LiClO4 as electrolyte material for battery Li-ion," IOP Conf. Ser. Mater. Sci. Eng., vol. 223, p. 012039, Jul. 2017, doi: 10.1088/1757-899X/223/1/012039.
[18] L.-F. Zhou, D. Yang, T. Du, H. Gong, and W.-B. Luo, "The Current Process for the Recycling of Spent Lithium Ion Batteries," Front. Chem., vol. 8, p. 578044, Dec. 2020, doi: 10.3389/fchem.2020.578044.
[19] Y. Yao, M. Zhu, Z. Zhao, B. Tong, Y. Fan, and Z. Hua, "Hydrometallurgical Processes for Recycling Spent Lithium-Ion Batteries: A Critical Review," ACS Sustain. Chem. Eng., vol. 6, no. 11, pp. 13611–13627, Nov. 2018, doi: 10.1021/acssuschemeng.8b03545.
[20] X. Chen, H. Ma, C. Luo, and T. Zhou, "Recovery of valuable metals from waste cathode materials of spent lithium-ion batteries using mild phosphoric acid," J. Hazard. Mater., vol. 326, pp. 77–86, Mar. 2017, doi: 10.1016/j.jhazmat.2016.12.021.
[21] P. Meshram, B. D. Pandey, and T. R. Mankhand, "Process optimization and kinetics for leaching of rare earth metals from the spent Ni–metal hydride batteries," Waste Manag., vol. 51, pp. 196–203, May 2016, doi: 10.1016/j.wasman.2015.12.018.
[22] G. Zhang, Z. Du, Y. He, H. Wang, W. Xie, and T. Zhang, "A Sustainable Process for the Recovery of Anode and Cathode Materials Derived from Spent Lithium-Ion Batteries," Sustainability, vol. 11, no. 8, p. 2363, Apr. 2019, doi: 10.3390/su11082363.
[23] M. Yu, Z. Zhang, F. Xue, B. Yang, G. Guo, and J. Qiu, "A more simple and efficient process for recovery of cobalt and lithium from spent lithium-ion batteries with citric acid," Sep. Purif. Technol., vol. 215, pp. 398–402, May 2019, doi: 10.1016/j.seppur.2019.01.027.
rik, and B. J. Bladergroen, "Recovery and Recycling of Valuable Metals from Spent Lithium-Ion

[24] X. Chen, D. Kang, L. Cao, J. Li, T. Zhou, and H. Ma, "Separation and recovery of valuable metals from spent lithium ion batteries: Simultaneous recovery of Li and Co in a single step," Sep. Purif. Technol., vol. 210, pp. 690–697, Feb. 2019, doi: 10.1016/j.seppur.2018.08.072.
[25] G. Gao et al., "A Citric Acid/Na2S2O3 System for the Efficient Leaching of Valuable Metals from Spent Lithium-Ion Batteries," JOM, vol. 71, no. 10, pp. 3673–3681, Oct. 2019, doi: 10.1007/s11837-019-03629-y.
[26] M. Zhou, B. Li, J. Li, and Z. Xu, "Pyrometallurgical Technology in the Recycling of a Spent Lithium Ion Battery: Evolution and the Challenge," ACS EST Eng., vol. 1, no. 10, pp. 1369–1382, Oct. 2021, doi: 10.1021/acsestengg.1c00067.
[27] B. Huang, Z. Pan, X. Su, and L. An, "Recycling of lithium-ion batteries: Recent advances and perspectives," J. Power Sources, vol. 399, pp. 274–286, Sep. 2018, doi: 10.1016/j.jpowsour.2018.07.116.
[28] Y. Yang et al., "A Closed-Loop Process for Selective Metal Recovery from Spent Lithium Iron Phosphate Batteries through Mechanochemical Activation," ACS Sustain. Chem. Eng., vol. 5, no. 11, pp. 9972–9980, Nov. 2017, doi: 10.1021/acssuschemeng.7b01914.
[29] D. Pant and T. Dolker, "Green and facile method for the recovery of spent Lithium Nickel Manganese Cobalt Oxide (NMC) based Lithium ion batteries," Waste Manag., vol. 60, pp. 689–695, Feb. 2017, doi: 10.1016/j.wasman.2016.09.039.
[30] T. Tawonezvi, M. Nomnqa, L. Petrik, and B. J. Bladergroen, "Recovery and Recycling of Valuable Metals from Spent Lithium-Ion Batteries: A Comprehensive Review and Analysis," Energies, vol. 16, no. 3, p. 1365, Jan. 2023, doi: 10.3390/en16031365.
[31] Elizabeth Weise, "Cell phones' lithium ion batteries are exploding, causing trash fires." Accessed: Dec. 11, 2024. [Online]. Available: https://www.usatoday.com/story/tech/talkingtech/2018/05/18/cell-phones-lithium-ion-batteries-exploding-causing-trash-fires/619897002/
[32] J. Li, G. Wang, and Z. Xu, "Generation and detection of metal ions and volatile organic compounds (VOCs) emissions from the pretreatment processes for recycling spent lithium-ion batteries," Waste Manag., vol. 52, pp. 221–227, Jun. 2016, doi: 10.1016/j.wasman.2016.03.011.
[33] M. M. Torabian, M. Jafari, and A. Bazargan, "Discharge of lithium-ion batteries in salt solutions for safer storage, transport, and resource recovery," Waste Manag. Res. J. Sustain. Circ. Econ., vol. 40, no. 4, pp. 402–409, Apr. 2022, doi: 10.1177/0734242X211022658.
[34] S. Ojanen, M. Lundström, A. Santasalo-Aarnio, and R. Serna-Guerrero, "Challenging the concept of electrochemical discharge using salt solutions for lithium-ion batteries recycling," Waste Manag., vol. 76, pp. 242–249, Jun. 2018, doi: 10.1016/j.wasman.2018.03.045.
[35] R. Eyjolfsson, "Introduction," in Design and Manufacture of Pharmaceutical Tablets, Elsevier, 2015, pp. 1–28. doi: 10.1016/B978-0-12-802182-8.00001-5.
[36] A. Y. Goren, Y. K. Recepoğlu, and A. Khataee, "Language of response surface methodology as an experimental strategy for electrochemical wastewater treatment process optimization," in Artificial Intelligence and Data Science in Environmental Sensing, Elsevier, 2022, pp. 57–92. doi: 10.1016/B978-0-323-90508-4.00009-5.
[37] A. S. Thomareis and G. Dimitreli, "Techniques used for processed cheese characterization," in Processed Cheese Science and Technology, Elsevier, 2022, pp. 295–349. doi: 10.1016/B978-0-12-821445-9.00007-8.
[38] J. V. D. Perez, E. T. Nadres, H. N. Nguyen, M. L. P. Dalida, and D. F. Rodrigues, "Response surface methodology as a powerful tool to optimize the synthesis of polymer-based graphene oxide nanocomposites for simultaneous removal of cationic and anionic heavy metal contaminants," RSC Adv., vol. 7, no. 30, pp. 18480–18490, 2017, doi: 10.1039/C7RA00750G.
[39]M. Alipanah, A. K. Saha, E. Vahidi, H. Jin, Department of System and Industrial Engineering, University of Arizona, 1127 E. James E. Rogers Way, Tucson, Arizona 85721, United States, and Department of Mining and Metallurgical Engineering, Mackay School of Earth Sciences and Engineering, University of Nevada, 1664 N. Virginia Street, Reno, Nevada 89557, United States, "Value recovery from spent lithium-ion batteries: A review on technologies, environmental impacts, economics, and supply chain," Clean Technol. Recycl., vol. 1, no. 2, pp. 152–184, 2021, doi: 10.3934/ctr.2021008.

[40] R. Golmohammadzadeh, F. Rashchi, and E. Vahidi, "Recovery of lithium and cobalt from spent lithium-ion batteries using organic acids: Process optimization and kinetic aspects," Waste Manag., vol. 64, pp. 244–254, Jun. 2017, doi: 10.1016/j.wasman.2017.03.037.
[41] S. K. Behera, H. Meena, S. Chakraborty, and B. C. Meikap, "Application of response surface methodology (RSM) for optimization of leaching parameters for ash reduction from low-grade coal," Int. J. Min. Sci. Technol., vol. 28, no. 4, pp. 621–629, Jul. 2018, doi: 10.1016/j.ijmst.2018.04.014.
[42] M. G. Weldeslase, N. E. Benti, M. A. Desta, and Y. S. Mekonnen, "Maximizing biodiesel production from waste cooking oil with lime-based zinc-doped CaO using response surface methodology," Sci. Rep., vol. 13, no. 1, p. 4430, Mar. 2023, doi: 10.1038/s41598-023-30961-w.
[43] E. R. Dyartanti, H. Susanto, I. N. Widiasa, and A. Purwanto, "Response surface method (RSM) for optimization of ionic conductivity of membranes polymer electrolyte poly (vinylidene fluoride) (PVDF) with polyvinyl pyrrolidone (PVP) as pore forming agent," IOP Conf. Ser. Mater. Sci. Eng., vol. 206, p. 012052, Jun. 2017, doi: 10.1088/1757-899X/206/1/012052.
[44] A. Malekian and N. Chitsaz, "Concepts, procedures, and applications of artificial neural network models in streamflow forecasting," in Advances in Streamflow Forecasting, Elsevier, 2021, pp. 115–147. doi: 10.1016/B978-0-12-820673-7.00003-2.
[45] A. I. Khuri and J. A. Cornell, Response Surfaces: Designs and Analyses: Second Edition, 0 ed. Routledge, 2018. doi: 10.1201/9780203740774.
[46] M. Kazemian, S. Gandjalikhan Nassab, and E. Jahanshahi Javaran, "Comparative study of Box–Behnken and central composite designs to investigate the effective parameters of ammonia–water absorption refrigerant system," Proc. Inst. Mech. Eng. Part C J. Mech. Eng. Sci., vol. 235, no. 16, pp. 3095–3108, Aug. 2021, doi: 10.1177/0954406220959097.
[47] A. Czyrski and H. Jarzębski, "Response Surface Methodology as a Useful Tool for Evaluation of the Recovery of the Fluoroquinolones from Plasma—The Study on Applicability of Box-Behnken Design, Central Composite Design and Doehlert Design," Processes, vol. 8, no. 4, p. 473, Apr. 2020, doi: 10.3390/pr8040473.
[48] R. F. Gunst, R. H. Myers, and D. C. Montgomery, "Response Surface Methodology: Process and Product Optimization Using Designed Experiments," Technometrics, vol. 38, no. 3, p. 285, Aug. 1996, doi: 10.2307/1270613.
[49] H. Lee, Y.-T. Kim, and S.-W. Lee, "Optimization of the Electrochemical Discharge of Spent Li-Ion Batteries from Electric Vehicles for Direct Recycling," Energies, vol. 16, no. 6, p. 2759, Mar. 2023, doi: 10.3390/en16062759.
[50] H. Berg, Batteries for Electric Vehicles: Materials and Electrochemistry, 1st ed. Cambridge University Press, 2015. doi: 10.1017/CBO9781316090978.
[51] M. Liu et al., "Failure mechanism and behaviors of lithium-ion battery under high discharging rate condition," J. Energy Storage, vol. 101, p. 113811, Nov. 2024, doi: 10.1016/j.est.2024.113811.
[52] S. Liu, J. Chen, C. Zhang, L. Jin, and Q. Yang, "Experimental study on lithium-ion cell characteristics at different discharge rates," J. Energy Storage, vol. 45, p. 103418, Jan. 2022, doi: 10.1016/j.est.2021.103418.
[53] Michael. J. Lain and E. Kendrick, "Understanding the limitations of lithium ion batteries at high rates," J. Power Sources, vol. 493, p. 229690, May 2021, doi: 10.1016/j.jpowsour.2021.229690.
[54] Z. Fang et al., "Comparative study of chemical discharge strategy to pretreat spent lithium-ion batteries for safe, efficient, and environmentally friendly recycling," J. Clean. Prod., vol. 359, p. 132116, Jul. 2022, doi: 10.1016/j.jclepro.2022.132116.
[55] J. Xiao, J. Guo, L. Zhan, and Z. Xu, "A cleaner approach to the discharge process of spent lithium ion batteries in different solutions," J. Clean. Prod., vol. 255, p. 120064, May 2020, doi: 10.1016/j.jclepro.2020.120064.
[56] J. Shaw-Stewart et al., "Aqueous solution discharge of cylindrical lithium-ion cells," Sustain. Mater. Technol., vol. 22, p. e00110, Dec. 2019, doi: 10.1016/j.susmat.2019.e00110.
[57] W.-C. Chen, J.-D. Li, C.-M. Shu, and Y.-W. Wang, "Effects of thermal hazard on 18650 lithium-ion battery under different states of charge," J. Therm. Anal. Calorim., vol. 121, no. 1, pp. 525–531, Jul. 2015, doi: 10.1007/s10973-015-4672-3.

[58] Y.-W. Lai, K.-H. Chi, Y.-H. Chung, S.-W. Liao, and C.-M. Shu, "Thermal runaway characteristics of 18650 lithium-ion batteries in various states of charge," J. Therm. Anal. Calorim., vol. 149, no. 19, pp. 10477–10486, Oct. 2024, doi: 10.1007/s10973-023-12867-x.
[59] G. Liu and L. Zhang, "Research on the Thermal Characteristics of an 18650 Lithium-Ion Battery Based on an Electrochemical–Thermal Flow Coupling Model," World Electr. Veh. J., vol. 12, no. 4, p. 250, Nov. 2021, doi: 10.3390/wevj12040250.
[60] Y. Chen, "Recent advances of overcharge investigation of lithium-ion batteries," Ionics, vol. 28, no. 2, pp. 495–514, Feb. 2022, doi: 10.1007/s11581-021-04331-3.
[61] D. Ren, X. Feng, L. Lu, X. He, and M. Ouyang, "Overcharge behaviors and failure mechanism of lithium-ion batteries under different test conditions," Appl. Energy, vol. 250, pp. 323–332, Sep. 2019, doi: 10.1016/j.apenergy.2019.05.015.
[62] H. Wang, Y. Liu, M. Jiang, and Q. Zhang, "A review of over-discharge protection through prelithiation in working lithium-ion batteries," J. Energy Chem., vol. 101, pp. 437–452, Feb. 2025, doi: 10.1016/j.jechem.2024.09.050.
[63] Erteza Tawsif Efaz, Abdullah Al Mamun, and MD. Rafsan Khan, "Development of Lithium Ion Battery with Overcharge and Deep Discharge Protection," Int. J. Sci. Eng. Res., vol. 8, no. 10, pp. 1677–1682, Oct. 2017.
[64] J. Jaguemont and F. Bardé, "A critical review of lithium-ion battery safety testing and standards," Appl. Therm. Eng., vol. 231, p. 121014, Aug. 2023, doi: 10.1016/j.applthermaleng.2023.121014.
[65] Rifat Farzana, Ravindra Rajarao, Pravas Ranjan Behera, Kamrul Hassan, and Veena Sahajwalla, "Zinc Oxide Nanoparticles from Waste Zn-C Battery via Thermal Route: Characterization and Properties," Sep. 2018, doi: https://doi.org/10.3390/nano8090717.
[66] D. Amalia, P. Singh, W. Zhang, and A. N. Nikoloski, "Discharging of Spent Cylindrical Lithium-Ion Batteries in Sodium Hydroxide and Sodium Chloride for a Safe Recycling Process," JOM, vol. 75, no. 11, pp. 4946–4957, Nov. 2023, doi: 10.1007/s11837-023-06093-x.
[67] M. Danko, J. Adamec, M. Taraba, and P. Drgona, "Overview of batteries State of Charge estimation methods," Transp. Res. Procedia, vol. 40, pp. 186–192, 2019, doi: 10.1016/j.trpro.2019.07.029.
[68] S. Bhattacharya, "Central Composite Design for Response Surface Methodology and Its Application in Pharmacy," in Response Surface Methodology in Engineering Science, P. Kayaroganam, Ed., IntechOpen, 2021. doi: 10.5772/intechopen.95835.
[69] J. Zhu et al., "Investigation of lithium-ion battery degradation mechanisms by combining differential voltage analysis and alternating current impedance," J. Power Sources, vol. 448, p. 227575, Feb. 2020, doi: 10.1016/j.jpowsour.2019.227575.
[70] H. Rouhi, E. Karola, R. Serna-Guerrero, and A. Santasalo-Aarnio, "Voltage behavior in lithium-ion batteries after electrochemical discharge and its implications on the safety of recycling processes," J. Energy Storage, vol. 35, p. 102323, Mar. 2021, doi: 10.1016/j.est.2021.102323.
[71] J. Tian, Y. Fan, T. Pan, X. Zhang, J. Yin, and Q. Zhang, "A critical review on inconsistency mechanism, evaluation methods and improvement measures for lithium-ion battery energy storage systems," Renew. Sustain. Energy Rev., vol. 189, p. 113978, Jan. 2024, doi: 10.1016/j.rser.2023.113978.
[72] S. Shrestha, B. Wang, and P. Dutta, "Nanoparticle processing: Understanding and controlling aggregation," Adv. Colloid Interface Sci., vol. 279, p. 102162, May 2020, doi: 10.1016/j.cis.2020.102162.
[73] L. Sun, G. Li, and F. You, "Combined internal resistance and state-of-charge estimation of lithium-ion battery based on extended state observer," Renew. Sustain. Energy Rev., vol. 131, p. 109994, Oct. 2020, doi: 10.1016/j.rser.2020.109994.
[74] Muhammad Fikri Irsyad Mat Razi, Zul Hilmi Che Daud, Zainab Asus, Izhari Izmi Mazali, Mohd Ibtisyam Ardani, and Mohd Kameil Abdul Hamid, "A Review of Internal Resistance and Temperature Relationship, State of Health and Thermal Runaway for Lithium-Ion Battery Beyond Normal Operating Condition," J. Adv. Res. Fluid Mech. Therm. Sci., vol. 88, no. 2, pp. 123–132, Nov. 2021, doi: 10.37934/arfmts.88.2.123132.

[75] F. Feng, X. Hu, L. Hu, F. Hu, Y. Li, and L. Zhang, "Propagation mechanisms and diagnosis of parameter inconsistency within Li-Ion battery packs," Renew. Sustain. Energy Rev., vol. 112, pp. 102–113, Sep. 2019, doi: 10.1016/j.rser.2019.05.042.
[76] F. T. Krauss, I. Pantenburg, and B. Roling, "Transport of Ions, Molecules, and Electrons across the Solid Electrolyte Interphase: What Is Our Current Level of Understanding?," Adv. Mater. Interfaces, vol. 9, no. 8, p. 2101891, Mar. 2022, doi: 10.1002/admi.202101891.
[77] S.-Y. Sun, X.-Q. Zhang, Y.-N. Wang, J.-L. Li, Z. Zheng, and J.-Q. Huang, "Understanding the transport mechanism of lithium ions in solid-electrolyte interphase in lithium metal batteries with liquid electrolytes," Mater. Today, vol. 77, pp. 39–65, Aug. 2024, doi: 10.1016/j.mattod.2024.06.001.
[78] M. Zhou, Y. Chen, G. Fang, and S. Liang, "Electrolyte/electrode interfacial electrochemical behaviors and optimization strategies in aqueous zinc-ion batteries," Energy Storage Mater., vol. 45, pp. 618–646, Mar. 2022, doi: 10.1016/j.ensm.2021.12.011.
[79] W. Zhang, X. Chen, Y. Wang, L. Wu, and Y. Hu, "Experimental and Modeling of Conductivity for Electrolyte Solution Systems," ACS Omega, vol. 5, no. 35, pp. 22465–22474, Sep. 2020, doi: 10.1021/acsomega.0c03013.
[80] E. Banguero, A. Correcher, Á. Pérez-Navarro, F. Morant, and A. Aristizabal, "A Review on Battery Charging and Discharging Control Strategies: Application to Renewable Energy Systems," Energies, vol. 11, no. 4, p. 1021, Apr. 2018, doi: 10.3390/en11041021.
[81] Y. Fu, Z. Gu, Q. Gan, and Y.-W. Mai, "A review on the ionic conductivity and mechanical properties of composite polymer electrolytes (CPEs) for lithium batteries: Insights from the perspective of polymer/filler composites," Mater. Sci. Eng. R Rep., vol. 160, p. 100815, Sep. 2024, doi: 10.1016/j.mser.2024.100815.
[82] M. R. Dunkin, S. T. King, K. J. Takeuchi, E. S. Takeuchi, L. Wang, and A. C. Marschilok, "Improved ionic conductivity and battery function in a lithium iodide solid electrolyte via particle size modification," Electrochimica Acta, vol. 388, p. 138569, Aug. 2021, doi: 10.1016/j.electacta.2021.138569.
[83] N. Nikfarjam, P. T. Coman, C. Free, P. Ziehl, M. Sadati, and R. E. White, "Advancing ionic conductivity in solid electrolytes: Insights from polymerization-induced phase separation and microstructural optimization," J. Energy Storage, vol. 93, p. 112287, Jul. 2024, doi: 10.1016/j.est.2024.112287.
[84] Tom Weideman, "3.2: Resistance and Energy Dissipation," Physics LibreTexts. Accessed: Dec. 11, 2024. [Online]. Available: https://phys.libretexts.org/Courses/University_of_California_Davis/UCD%3A_Physics_9C__Electricity_and_Magnetism/3%3A_Direct_Current_Circuits/3.2%3A_Resistance_and_Energy_Dissipation
[85] hari Kraber, "R-Squared Mysteries Solved," StatEase. Accessed: Jan. 29, 2025. [Online]. Available: https://www.statease.com/blog/r-squared-mysteries-solved/
[86] StatEase, "Adequate Precision," StatEase. Accessed: Jan. 29, 2025. [Online]. Available: https://www.statease.com/docs/latest/right-click-help/anova/anova-adequate-precision/
[87] R. Ghelich, M. R. Jahannama, H. Abdizadeh, F. S. Torknik, and M. R. Vaezi, "Central composite design (CCD)-Response surface methodology (RSM) of effective electrospinning parameters on PVP-B-Hf hybrid nanofibrous composites for synthesis of HfB2-based composite nanofibers," Compos. Part B Eng., vol. 166, pp. 527–541, Jun. 2019, doi: 10.1016/j.compositesb.2019.01.094.
[88] D. Asante-Sackey, S. Rathilal, L. V. Pillay, and E. Kweinor Tetteh, "Ion Exchange Dialysis for Aluminium Transport through a Face-Centred Central Composite Design Approach," Processes, vol. 8, no. 2, p. 160, Jan. 2020, doi: 10.3390/pr8020160.
[89] StatEase, "Desirability Function," StatEase. Accessed: Jan. 29, 2025. [Online]. Available: https://www.statease.com/docs/v23.1/contents/optimization/desirability-function/?utm_source=chatgpt.com
[90] M. A. Bezerra et al., "Simultaneous optimization of multiple responses and its application in Analytical Chemistry – A review," Talanta, vol. 194, pp. 941–959, Mar. 2019, doi: 10.1016/j.talanta.2018.10.088.